Sensor and Simulation Notes

Note 176

May 1973

Natural Modes of Two Collinear Cylinders

Lennart Marin
Dikewood Corporation, Westwood Research Branch
Los Angeles, California

Abstract

The natural frequencies and the current distribution of the natural
modes of two, perfectly conducting, solid, finite, collinear cylinders are
determined.   The analysis is based on the magnetic-field integral equation
specialized to the case of rotational symmetry.   The results are presented
in form of graphes and tables for the natural frequencies and the current
and charge distributions of the natural modes.

I. Introduction

The singularity expansion method (SEM) for solving transient electro-
magnetic interaction problems was first proposed by Baum in [1]. This method
is based on the analytical properties of the field in the complex frequency(s)
plane. The singularity expansion method prompted the study that is undertaken
in [2] of the analytical properties in the complex s plane of the field
scattered from a perfectly conducting, finite body. It is shown in [2] that
the operator inverse to the integral operator of the magnetic-field formulation
is an analytic operator-valued function in the complex frequency plane except
at certain points in the left half-plane where it has poles. A representation
of the inverse operator in terms of the natural modes and frequencies is also
given in [2]. Some analytical properties of the field scattered from imperfectly
conducting bodies and perfectly conducting bodies located in a parallel plate
region are discussed in [3]. The singularity expansion method for the special
case of first order poles is treated in great detail in [4].

One of the advantages of the singularity expansion method as compared to
other more conventional methods is that it provides a means of characterizing
the electromagnetic properties of a body with a set of complex numbers (the
natural frequencies) and two sets of modal functions. These quantities are
uniquely determined by the body itself and do not depend, for example, on the
incident field. Once these quantities are known a wide variety of scattering
and antenna problems can be solved without having to solve any boundary value
problems. The singularity expansion method is therefore more desirable than
other more conventional methods for two reasons: (1) it provides more physical
insight into the problem and (2) it has many computational advantages.

Recently, the natural frequencies and modes have been calculated numerically
for certain differently shaped, perfectly conducting bodies. The electric-field
integral equation is used in [5] to numerically obtain the natural modes of a
perfectly conducting thin wire. Some approximate analytical results regarding
the locations of the natural frequencies of a thin wire are derived in [6]
from an approximate solution of the electric-field integral equation. The
natural frequencies and modes of a perfectly conducting sphere are calculated
in [7] by using an eigenfunction expansion of the scattered field. In [8] the
natural modes of a prolate spheroid are obtained by applying the theory developed

2

in [2] to perfectly conducting, rotationally symmetric bodies.

The expansion of the scattered field in natural modes is very expedient when evaluating the fields for moderate and large times. For example, when a step-function plane wave is impinging on a perfectly conducting body a reasonable number of terms is needed to describe the induced current density for times after the wavefront has passed the body. However, for times such that only part of the scattering body is illuminated the convergence of the series is rather poor. Another method which is more useful for early times is presented in [9].

So far all numerical calculations of natural modes have been limited to simple, isolated, perfectly conducting[5]-[8] or resistively loaded[11] bodies. Some preliminary results for the two-body problem are reported in [10]. The purpose of this note is to study the natural modes of two, perfectly conducting, solid, finite, collinear cylinders when the size of the cylinders is kept constant but the distance between them varies. From image theory it is clear that part of the natural modes of two cylinders are those of one cylinder above a perfectly conducting plane.

In Section II we derive an integral equation for the total current on each cylinder. The natural modes are then obtained from the nontrivial solutions of the homogeneous integral equation. In general, numerical methods have to be used to find these solutions. However, in the limiting case as the radius of each cylinder becomes vanishingly small the integral equation can be solved analytically. In this case, all the natural frequencies are located on the imaginary axis of the s-plane.

The results of the numerical calculations are presented in Section IV in graphical form for the locations of the natural frequencies in the complex frequency plane as well as the spatial variation of the current and charge distributions of the natural modes. Particular attention is given to the variation of the two fundamental modes as the distance between the cylinders varies. It is found in [5] through [8] that the natural frequencies of one perfectly conducting body seem to occur in layers in the complex frequency plane. The natural frequencies of two scattering bodies do not in general possess this property.

3

II. Integral Equation for the Cylinder Current

In this section we will derive an integral equation describing scattering from two perfectly conducting, solid, finite collinear cylinders (see Figure 1). Following the approach in [12] we have the following integral equation for the ϕ-symmetric part of the tangential component of the magnetic field, $H_\phi(\rho,z)$, on the surfaces of the two cylinders

$$f(\rho,z)H_\phi(\rho,z) + \int_0^a [K_1(\rho,z,\rho',d)H_\phi(\rho',d) + K_1(\rho,z,\rho',-d)H_\phi(\rho',-d)$$

$$- K_1(\rho,z,\rho',b)H_\phi(\rho',b) - K_1(\rho,z,\rho',-b)H_\phi(\rho',-b)]\rho'd\rho' - \int_d^b [K_2(\rho,z,a,z')H_\phi(a,z')$$

$$+ K_2(\rho,z,a,-z')H_\phi(a,-z')]dz' = H_\phi^{inc}(\rho,z), \qquad (\rho,z) \in S_1 \text{ or } S_2. \qquad (1)$$

Here,

$$f(\rho,z) = \begin{cases} 1/2, & \text{if } (|\rho - a| + |z \pm d|)(|\rho - a| + |z \pm b|) \neq 0 \\ 1/4, & \text{if } (|\rho - a| + |z \pm d|)(|\rho - a| + |z \pm b|) = 0 \end{cases} \qquad (2)$$

$$K_1(\rho,z,\rho',z') = \frac{\partial}{\partial z'}[G(\rho,z,\rho',z';\gamma)] \qquad (3)$$

$$K_2(\rho,z,\rho',z') = -\frac{\partial}{\partial \rho'}[\rho'G(\rho,z,\rho',z';\gamma)] \qquad (4)$$

$$G(\rho,z,\rho',z';\gamma) = (4\pi)^{-1}\int_0^{2\pi} R^{-1}\exp(-\gamma R)\cos\psi d\psi \qquad (5)$$

$$R = [\rho^2 + \rho'^2 - 2\rho\rho'\cos\psi + (z - z')^2]^{1/2} \qquad (6)$$
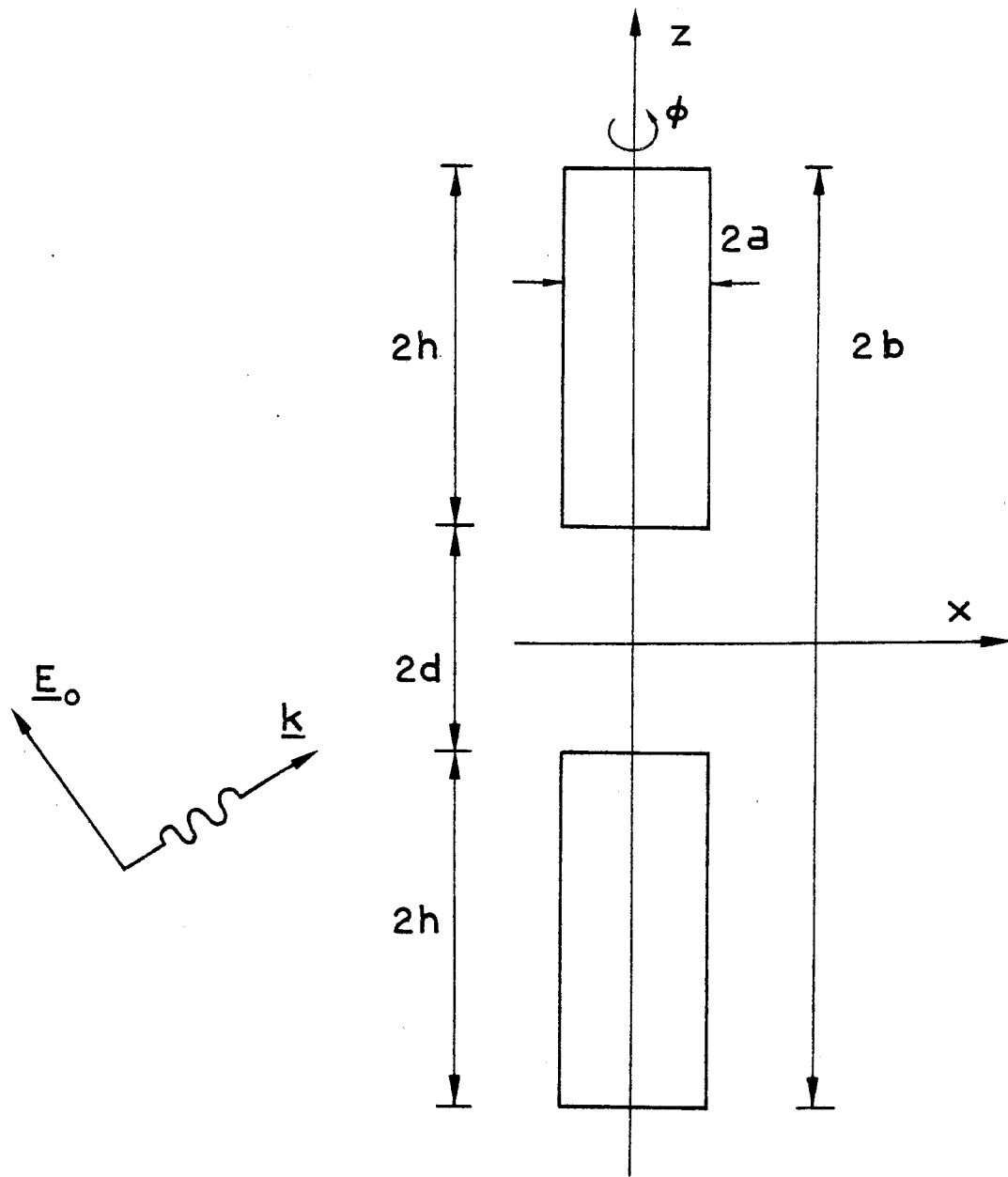
Figure 1. Electromagnetic interaction of two collinear cylinders and a plane wave.

and $S_1(S_2)$ denotes the surface of the top (bottom) cylinder.

In terms of the total current, $I(\rho,z)$, defined by

$$I(\rho,z) = 2\pi\rho H_\phi(\rho,z) \tag{7}$$

equation (1) becomes

$$f(\rho,z)I(\rho,z) + \int_0^a \rho[K_1(\rho,z,\rho',d)I(\rho',d) + K_1(\rho,z,\rho',-d)I(\rho',-d)$$

$$- K_1(\rho,z,\rho',b)I(\rho',b) - K_1(\rho,z,\rho',-b)I(\rho',-b)]d\rho' - \int_d^b \rho[K_2(\rho,z,a,z')I(a,z')$$

$$+ K_2(\rho,z,a,-z')I(a,-z')]dz' = 2\pi\rho H_\phi^{inc} \tag{8}$$

To solve the integral equation (8) we first transform it into two somewhat simpler integral equations. Split $I(\rho,z)$ and $H_\phi^{inc}(\rho,z)$ into their even and odd parts:

$$I(\rho,z) = I^+(\rho,z) + I^-(\rho,z)$$

$$H_\phi^{inc}(\rho,z) = H_+^{inc}(\rho,z) + H_-^{inc}(\rho,z) \tag{9}$$

where

$$I^\pm(\rho,z) = [I(\rho,z) \pm I(\rho,-z)]/2 \tag{10}$$

and, similarly, for $H_+^{inc}(\rho,z)$ and $H_-^{inc}(\rho,z)$. The functions $I^+(\rho,z)$ and $I^-(\rho,z)$ satisfy the following set of uncoupled integral equations

$$f(\rho,z)I^+(\rho,z) + \int_0^a \rho[K_1^+(\rho,z,\rho',d)I^+(\rho',d) - K_1^+(\rho,z,\rho',b)I^+(\rho',b)]d\rho'$$

$$- \int_d^b \rho a^{-1}K_2^+(\rho,z,a,z')I^+(a,z')dz' = 2\pi\rho H_+^{inc}(\rho,z), \quad (\rho,z) \in S_1 \quad (11)$$

$$f(\rho,z)I^-(\rho,z) + \int_0^a \rho[K_1^-(\rho,z,\rho',d)I^-(\rho',d) - K_1^-(\rho,z,\rho',b)I^-(\rho',b)]d\rho'$$

$$- \int_d^b \rho a^{-1}K_2^-(\rho,z,a,z')I^-(a,z')dz' = 2\pi\rho H_-^{inc}(\rho,z), \quad (\rho,z) \in S_1 \quad (12)$$

where $K_1^\pm(\rho,z,\rho',z')$ and $K_2^\pm(\rho,z,\rho',z')$ are determined by substituting $G^\pm(\rho,z,\rho',z';\gamma)$ into (3) and (4) and

$$G^\pm(\rho,z,\rho',z';\gamma) = (4\pi)^{-1} \int_0^{2\pi} [R_+^{-1} \exp(-\gamma R_+) \pm R_-^{-1} \exp(-\gamma R_-)]\cos \psi d\psi$$

$$\tag{13}$$

$$R_\pm = [\rho^2 + \rho'^2 - 2\rho\rho' \cos \psi + (z \pm z')^2]^{1/2}.$$

The integral equation (12) is identical to the integral equation (6) in [12] describing scattering from a perfectly conducting post above a ground plane.

Equations (11) and (12) constitute the mathematical formulation of the electromagnetic scattering problem. In the next section we will go on to discuss the properties of the solution of the integral equations (11) and (12).

7

III. Numerical Calculation of the Natural Modes

In this section we will discuss briefly how to obtain the natural frequencies and the current distribution of the natural modes.

The kernels $K_1^{\pm}(\rho,z,\rho',z')$ and $K_2^{\pm}(\rho,z,\rho',z')$ that appear in (11) and (12) have a logarithmic singularity at $\rho = \rho'$, $z = z'$. Moreover, $K_1^{\pm}(\rho,z,\rho',z')$ and $K_2^{\pm}(\rho,z,\rho',z')$ are square integrable and hence they are of Hilbert-Schmidt type. Therefore, poles are the only singularities in the complex γ-plane of the solutions of the integral equations (11) and (12) provided that $H_+^{inc}(\rho,z)$ and $H_-^{inc}(\rho,z)$ are analytic functions in the entire γ-plane. In [2] it has been shown that the locations of these poles, i.e., the natural frequencies, can be determined from the eigenvalue problem: Find the values of γ, γ_n^+ and γ_n^- respectively, such that the homogeneous integral equations have nontrivial solutions

$$A_+(\gamma_n^+)I_n^+ = 0$$

$$A_-(\gamma_n^-)I_n^- = 0$$

(14)

Here, $A_+(\gamma)$ and $A_-(\gamma)$ are integral operators defined by the integral equations (11) and (12), respectively. It has also been shown that there exists $H_n^{\pm}$ such that[2]

$$A_+^T(\gamma_n^+)H_n^+ = 0$$

$$A_-^T(\gamma_n^-)H_n^- = 0$$

(15)

where $A^T(\gamma) = A^{\dagger *}(\gamma)$, the star denotes complex conjugation and $A^{\dagger}$ is the adjoint operator of A. The quantity $s_n^{\pm} = c\gamma_n^{\pm}$ is called a natural frequency of the body and $I_n^{\pm}$ the current distribution of a natural mode.

In order to determine the natural modes it is necessary to solve the homogeneous equations (11) and (12). It is not possible in the general case to solve these equations analytically so numerical mehtods have to be used.

8

It should, however, be pointed out that the natural modes of a perfectly conducting cylindrical tube can be determined analytically in the limit as the diameter-to-length ratio of the tube becomes very small (see Appendix A). The integral equations (11) and (12) can be approximated by matrix equations[8],[12]. Thus, in the matrix approximation (14) gives the following set of algebraic equations

$$M_{\pm}(\gamma_n^{\pm})\overline{I}_n^{\pm} = 0 \tag{16}$$

where $M_{\pm}(\gamma)$ is a N×N matrix and $\overline{I}_n^{\pm}$ is a column vector determining the current at N sample points (see Figure 2). The method used to determine the elements in $M_{\pm}(\gamma)$ from the integral operator $A_{\pm}(\gamma)$ is presented in [8]. Thus, by finding $\gamma_n^{\pm}$ from

$$\det\{M_{\pm}(\gamma_n^{\pm})\} = 0 \tag{17}$$

and the corresponding nontrivial solutions $\overline{I}_n^{\pm}$ and $\overline{H}_n^{\pm}$ from

$$M_{\pm}(\gamma_n^{\pm})\overline{I}_n^{\pm} = 0$$

$$M_{\pm}^T(\gamma_n^{\pm})\overline{H}_n^{\pm} = 0 \tag{18}$$

we can determine $I_n^{\pm}$ and $H_n^{\pm}$ numerically. A detailed analysis of how to determine $\gamma_n^{\pm}$, $\overline{I}_n^{\pm}$, $\overline{H}_n^{\pm}$ from (17) and (18) is presented in [8].

The segments into which each cylinder is divided for the numerical calculations are shown in Figure 2. The cylindrical surface is divided into 31 segments (c.f. Figure 2). In the special case where d = 0 we, of course, omitted the lower planar surface. The numerical calculations were performed for a/h = .1 and various d/h values. The kernel in the integral equation is an exponentially growing function of $R_{\pm} = [\rho^2 + \rho'^2 - 2\rho\rho' \cos \psi - (z \pm z')^2]^{1/2}$ when γ belongs to the left half-plane. This exponential growth introduces numerical inaccuracies so we had to limit the numerical calculations to d/h ≤ 1.

9

An iterative method similar to the Newton-Raphson method of finding zeros of real functions was used to find the natural frequencies. Each iteration was started by an initial guess of the natural frequency and stopped when the difference of γd between two consecutive iterations was less than 10^{-4}. The ratio of $\det\{M(\gamma)\}$ at the end point to that at the starting point of each iteration was less than 10^{-5}. It was also found numerically that all zeros of $\det\{M(\gamma)\}$ are simple zeros.

We wish to point out that the interior resonances of one cylinder can also be obtained from (1) although the integral equation was originally derived for the exterior scattering problem. This fact provides a useful check on the numerical calculations.

In the next section we will present the results of the numerical calculations obtained by using the methods discussed in this section.
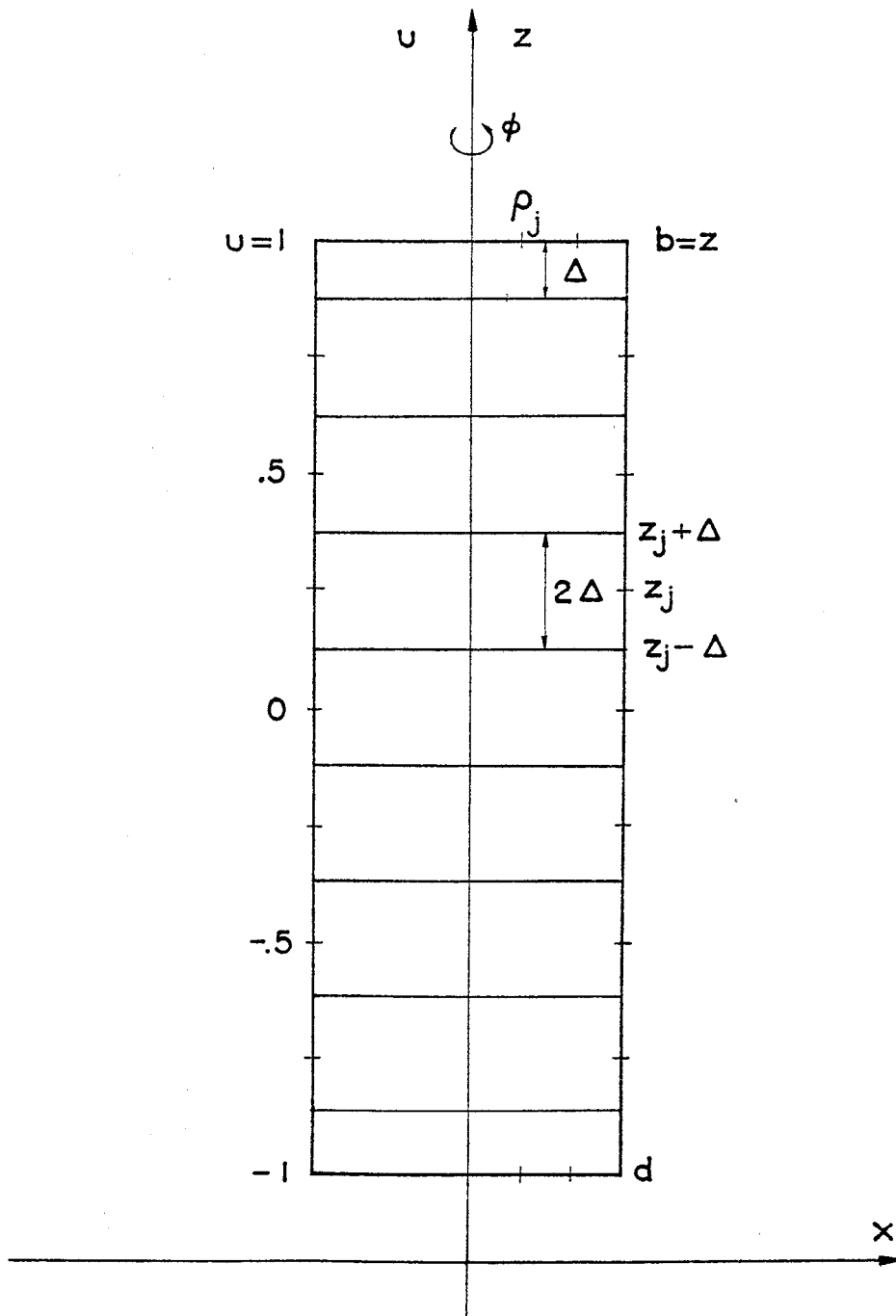
Figure 2.   The zones and sample points used in the numerical quadrature of
the integral equation.

IV. Numerical Results

In this section we will present the results of the numerical calculations that were obtained with the aid of a CDC 6600 computer. We will first present the results that were obtained for the variation with the diameter-to-length ratio of the natural frequencies and the current and charge distributions of some of the natural modes of one perfectly conducting, solid cylinder. Then, we will present the calculations on certain important quantities for two collinear cylinders when the size of each cylinder is kept constant but the distance between them varies.

A. Natural Modes of One Cylinder

The result of the search in the complex γ-plane for the natural frequencies of one cylinder is presented in Figures 3 and 4. The H-field integral equation was used to numerically determine the natural frequencies when a/h = .1, .05 whereas the E-field integral equation was used to determine these quantities numerically[5] for a/h = .01 and analytically for a/h → 0. All calculations were concentrated on the first layer since previous studies[5,8] show that this layer is the most important one. We note that the absolute value of the real part of γh is a monotonically increasing function of a when h is fixed. This means that the Q-value of each mode is a decreasing function of a when h is fixed. The notation "even" and "odd" in Figure 3 refers to the symmetry proper-ties about z = 0 of the current distribution of the natural mode. (c.f. [14] where the notation "antisymmetric" and "symmetric", respectively, has been used). In Table 1 we have tabulated certain natural frequencies of one cylinder for different values of a/h.

The magnitude of the current and charge distributions of first-layered natural modes of one cylinder are depicted in Figures 5 through 7. In these figures we have chosen to normalize the current density, j_n, so that its absolute value is less than or equal to one and that j_n is real and positive when $|j_n| = 1$. The continuity equation enables us to calculate the charge density, q_n, from the current density giving $q_n = j_n'/ch\gamma_n$. Here, the prime denotes differentiation with respect to u. The results for the charge distribution were obtained by performing a numerical differentiation of the current distribution. There-fore, we expect the results for the charge distribution to be less accurate that those for the current distribution. The phase variation of the current

12

and charge distribution of natural modes when $a/h = .05$ are presented in
Figure 8.

B. Natural Modes of Two Collinear Cylinders

The natural frequencies of two collinear cylinders are depicted in Figures 9
through 13. In obtaining these results the size of each cylinder was constant
($a/h = .1$) but the distance between the two cylinders varied. As mentioned
previously, due to numerical accuracy problems, the calculations were limited to
$d/h < 1$. The case where $d/h = \infty$ was, of course, obtained by considering one
cylinder in free space. In Figures 9 through 13 "even" and "odd" refer to the
symmetry properties about $z = 0$ of the z-component of the current density on
the two cylinders. For $d/h = \infty$ there is no interaction between the two cylinders
so that the natural frequencies for even and odd modes coincide in this case.
For $d/h = 1$ we observe that there are two natural frequencies in the vicinity
of the lowest natural frequency of one cylinder. One of these frequencies
corresponds to an even natural mode and the other to an odd natural mode. This
effect may be called mode splitting, since due to the interaction between the
two cylinders the lowest natural mode of one cylinder is split up into one even
and one odd natural mode of two cylinders. The loci of natural modes in the
complex frequency plane as the distance between the two cylinders varies are
rather complicated and we will return to some of these questions later. As d/h
varies from infinity to zero, we note from Figures 9 through 13 that the two
lowest natural frequencies vary between the lowest natural frequency of one
cylinder where $a/h = .1$ and the two lowest natural frequencies of one cylinder
where $a/h = .05$. Some natural frequencies are tabulated in Table 2.

The current and charge distributions of some natural modes are depicted in
Figures 14 through 18. We observe from these figures that the current and charge
distributions for even and odd modes almost coincide for $d/h = 1$, indicating
that the interaction between the two cylinders is very weak for these two modes.

C. Variation of the Lowest Natural Modes With d/h.

We now go on to study in detail the variation of the two lowest even and odd
natural modes with d/h.

The loci in the γ-plane of the first even and odd modes are depicted in
Figure 19. It can be seen from this figure that the interaction between the two

13

cylinders for even modes is a rapidly varying function of d/h for small values of d/h. This interaction between the cylinders is due to the capacitive coupling between the two cylinders. The capacitance of two cylinders is a quantity that varies rapidly with d/h for small values for d/h[13]. The coupling between the cylinders is very weak for odd modes since the current distribution of odd modes has a node at $z = 0$ when d/h = 0. The current and charge distributions of the lowest even and odd natural modes are graphed in Figures 20 and 21 for d/h = 0, .01, .1, .5, 1.

The variation of the "second" natural frequency with d/h is not so simple. In this case, the natural frequencies seems to belong to different branches. We have depicted 4 different branches in Figure 22. The question whether the natural frequency for d/h = ∞ can be viewed as belonging to any of these 4 branches has to be left unanswered. The spiraling behavior of the loci of the natural frequencies for two cylinders around the natural frequency of one cylinder has also been observed in the case of a thin wire arbitrarily oriented above a ground plane[10]. The current distributions for modes belonging to any of the 4 branches in Figure 22 are shown in Figures 23 through 30. It should be mentioned that different modes for fixed value of d/h have a more rapid variation the larger $\text{Im}\{\gamma h\}$ is.

14

a/h = .1		a/h = .05		a/h = .01		a/h = 0	
Re{γh}	Im{γh}	Re{γh}	Im{γh}	Re{γh}	Im{γh}	Re{γh}	Im{γh}
−.234	1.255	−.194	1.334	−.126	1.456	0	1.571
−.409	2.688	−.316	2.809	−.181	2.981	0	3.142
−.549	4.088	−.393	4.228	−.223	4.507	0	4.712
−.727	5.635	−.507	5.823	−.259	6.048	0	6.283
−.890	7.081	−.581	7.285	−.284	7.574	0	7.854
−1.068	8.652	−.680	8.875	−.303	9.133	0	9.425
−1.292	10.169	−.760	10.357	−.320	10.659	0	10.996
−1.477	11.777	−.852	11.952	−.34	12.16	0	12.566
−1.651	13.515	−.942	13.450	−.35	13.69	0	14.137
−1.841	15.232	−1.030	15.051	−.36	15.22	0	15.708

Table 1. Natural frequencies of a perfectly conducting, solid, finite cylinder where a/h = .1, .05, .01, 0.

d/h = 0		d/h = .01		d/h = .1		d/h = 1		d/h = ∞	
Re{γh}	Im{γh}	Re{γh}	Im{γh}	Re{γh}	Im{γh}	Re{γh}	Im{γh}	Re{γh}	Im{γh}
-.097	.667	-.181	.884	-.289	1.083	-.237	1.300	-.222	1.253
-.158	1.405	-.157	1.398	-.152	1.350	-.218	1.216	-.222	1.253
-.196	2.114	-.265	2.262	-.463	2.388	-.337	2.640	-.409	2.688
-.254	2.912	-.252	2.898	-.246	2.798	-.458	2.793	-.409	2.688
-.290	3.643	-.340	3.736	-.568	3.738	-.741	3.756	-.549	4.088
-.340	4.438	-.338	4.417	-.332	4.264	-.431	4.126	-.549	4.088
-.380	5.179	-.415	5.242	-.635	5.125	-.643	4.415	-.727	5.635
-.426	5.976	-.423	5.948	-.418	5.740	-.690	5.260	-.727	5.635
-.471	6.725	-.494	6.766	-.684	6.546	-.518	5.647	-.890	7.081
-.515	7.525	-.512	7.490	-.506	7.226	-.726	6.063	-.890	7.081
-.566	8.286	-.577	8.308	-.729	8.000	-.691	6.778	-1.068	8.652
-.609	9.089	-.605	9.046	-.599	8.721	-.603	7.199	-1.068	8.652
-.667	9.866	-.667	9.870	-.778	9.483	-.754	7.682	-1.292	10.169
-.708	10.673	-.703	10.622	-.694	10.231	-.719	8.331	-1.292	10.169
-.771	11.476	-.759	11.460	-.829	10.999	-.667	8.773	-1.477	11.777
-.803	12.288	-.797	12.228	-.784	11.762	-.794	9.305	-1.477	11.777

Table 2. Natural frequencies of two, perfectly conducting, solid, finite, collinear cylinders where a/h = .1, and d/h = 0, .01, .1, 1, ∞.

The following tables summarize the different combinations of parameters for which numerical data are presented in Figures 3 through 30.

Figure	Quantity	a/h
3	Frequency	0, .01, .05, .1
4	Frequency	0 < a/h < .1
5	Current & Charge, Magnitude	.1
6	Current & Charge, Magnitude	.05
7	Current & Charge, Magnitude	0
8	Current & Charge, Phase	.05

Figure	Quantity	d/h
9	Frequency	0
10	Frequency	.01
11	Frequency	.1
12	Frequency	1
13	Frequency	∞
14	Current & Charge, Magnitude	0
15	Current & Charge, Magnitude	.01
16	Current & Charge, Magnitude	.1
17	Current & Charge, Magnitude	1
18	Current & Charge, Magnitude	∞

Figure	Quantity	Pole #	d/h	Symmetry*
19	Frequency	1	0 < d/h < 1	Even & Odd
20	Current & Charge	1	0, .01, .1, .5, 1	Even
21	Current & Charge	1	0, .1, .5, 1	Odd
22	Frequency	2	0 < d/h < 1	Even & Odd
23	Current & Charge	2	0, .1, .2, .26, .3	Even
24	Current & Charge	2	.3, .7, .9, 1	Odd
25	Current & Charge	2	.2, .26, .3, .5	Even
26	Current & Charge	2	.7, .8, .84, .9	Odd
27	Current & Charge	2	.2	Even & Odd
28	Current & Charge	2	.3	Even & Odd
29	Current & Charge	2	.7	Even & Odd
30	Current & Charge	2	.9	Even & Odd

*The notation + (-) is used in Section III for even (odd).
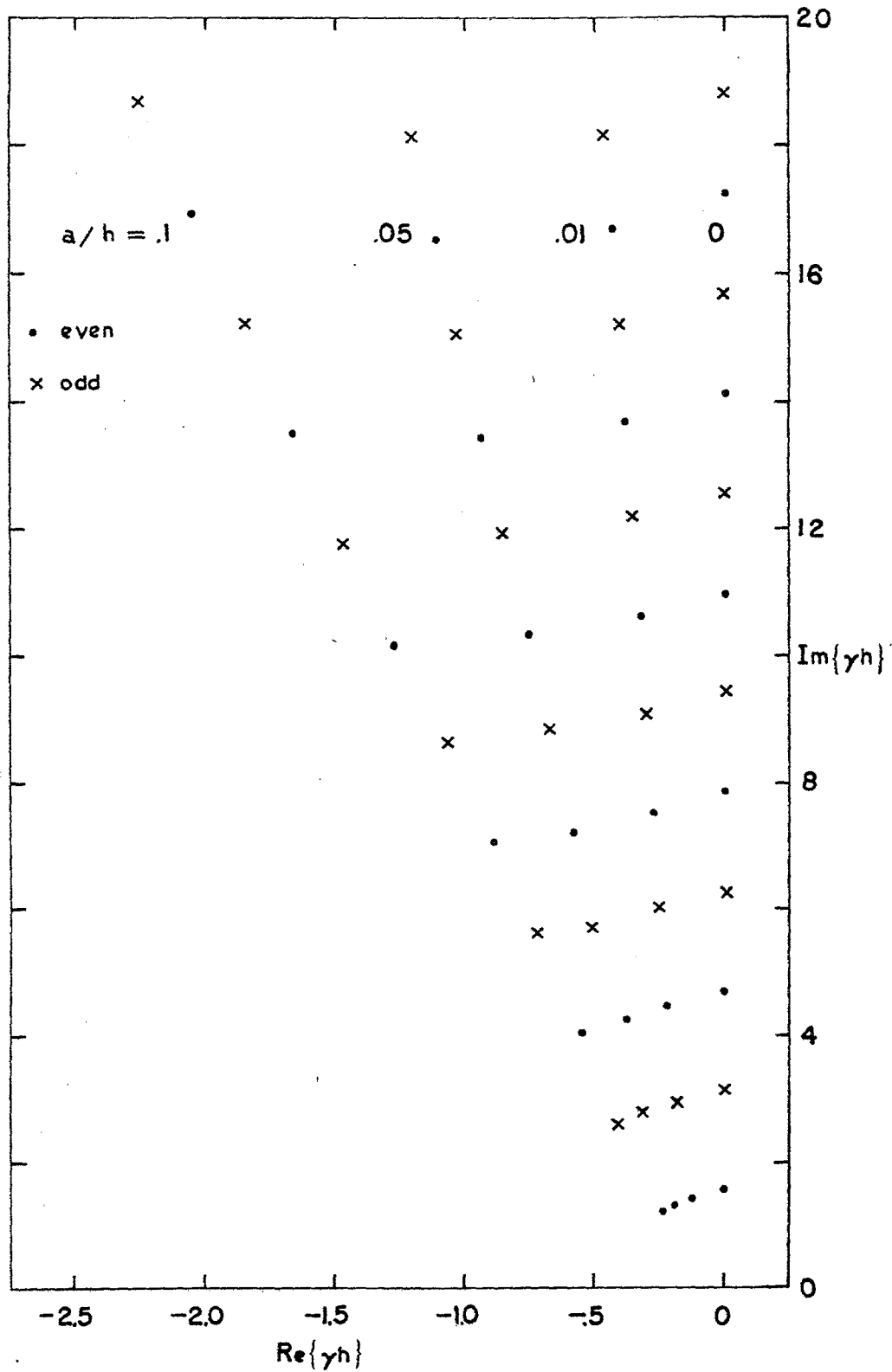
Figure 3. Natural frequencies of a cylinder for different diameter-to-length ratios.

18
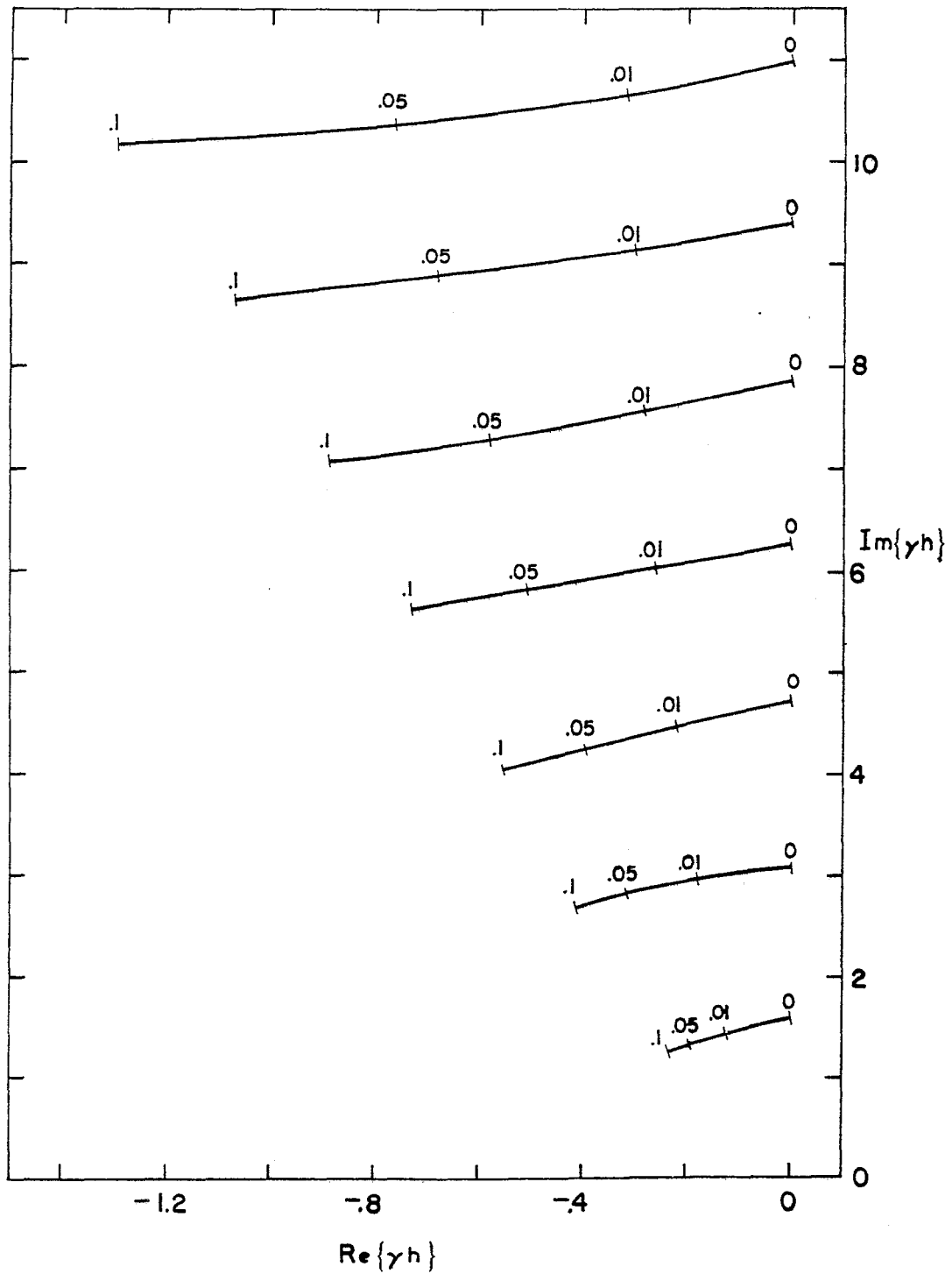
Figure 4. Loci of natural frequencies when 0 < a/h < .1. The location of the natural frequencies for a/h = 0, .01, .05, .1 is indicated on the curves.

19

Figure 5. The current and charge distributions of natural modes of a solid cylinder where a/h = .1.

20
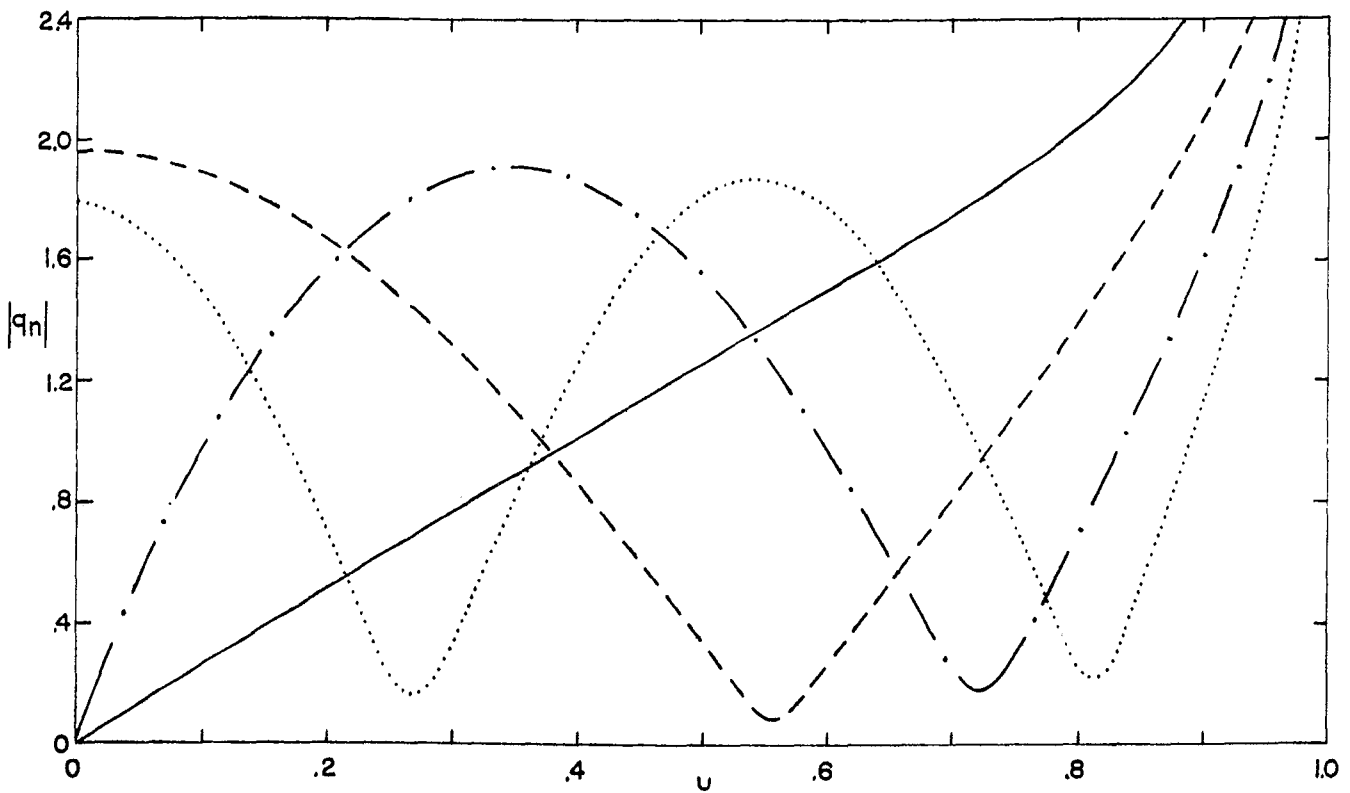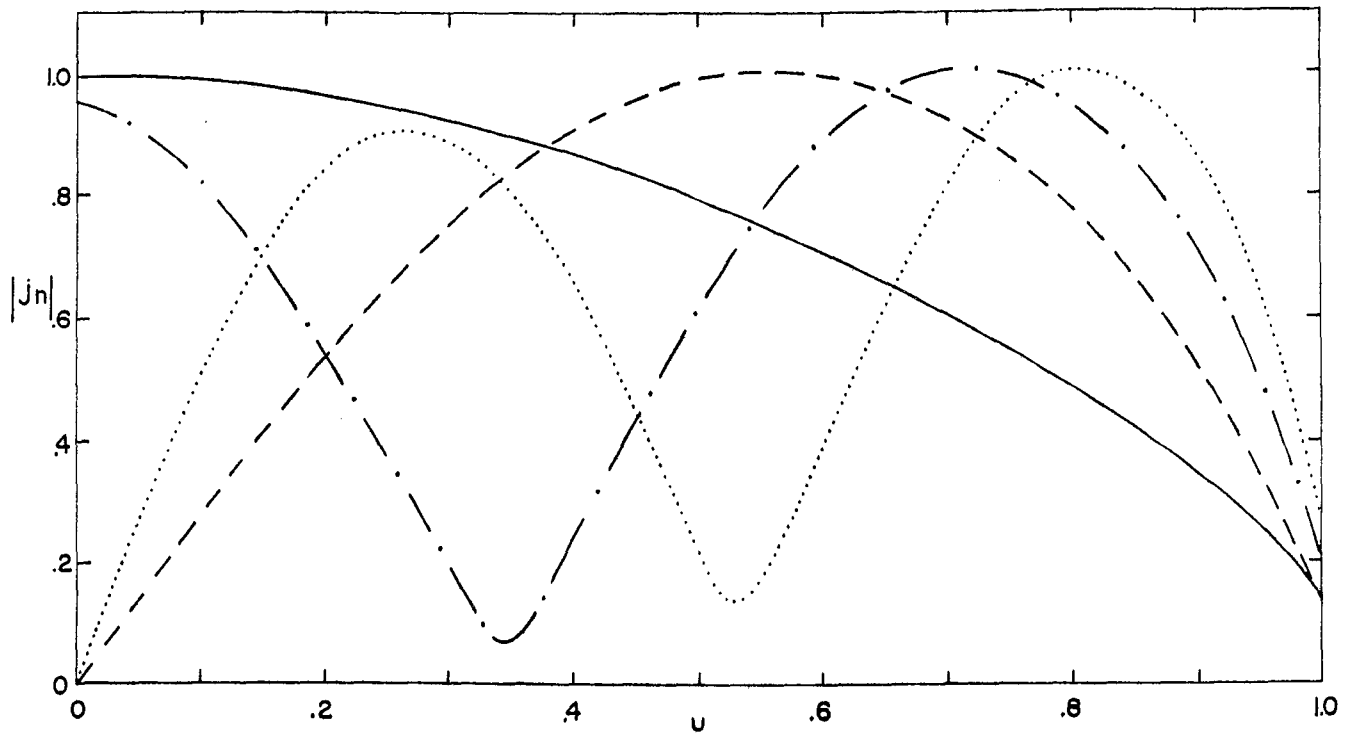
Figure 6. The current and charge distributions of natural modes of a solid cylinder where a/h = .05.
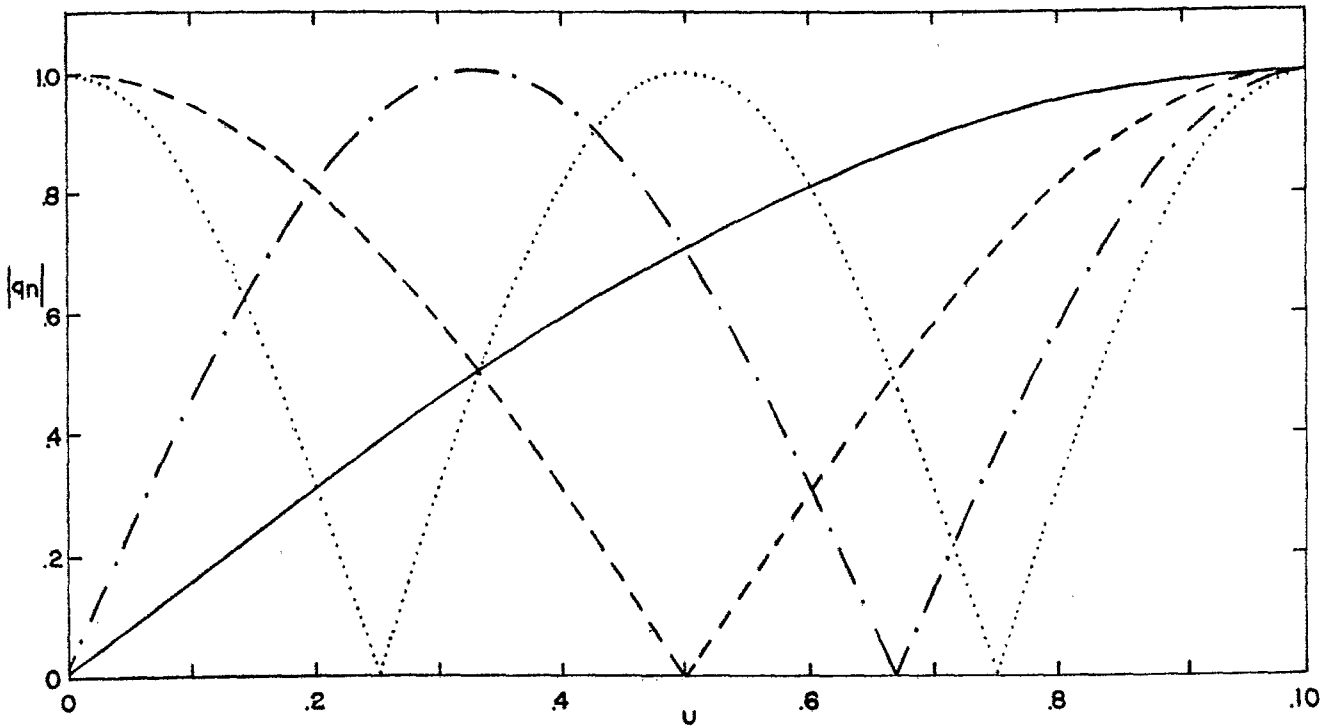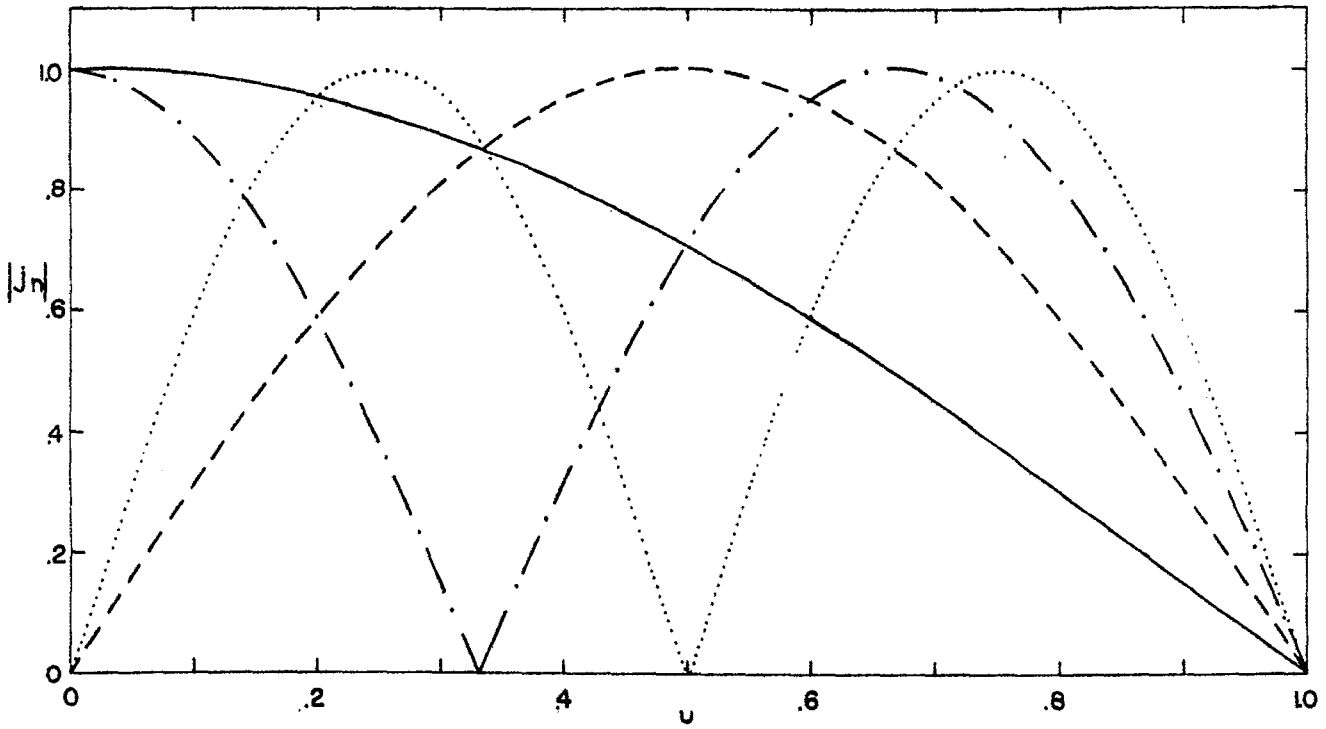
Figure 7. The current and charge distributions of natural modes of a solid
cylinder when a/h = 0.
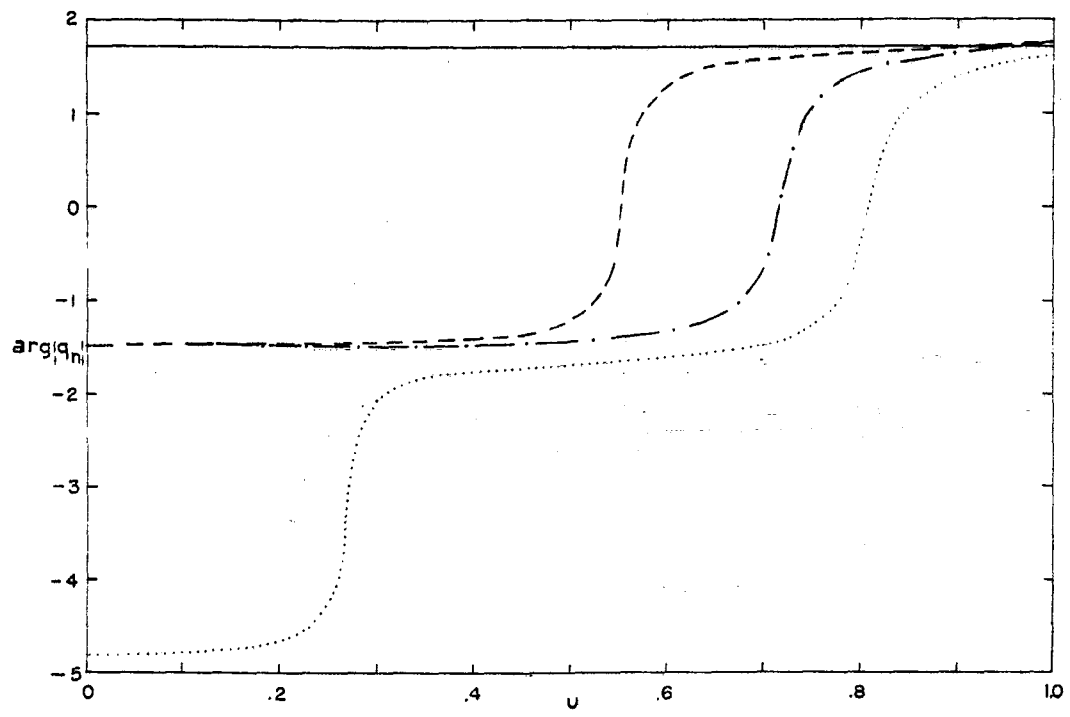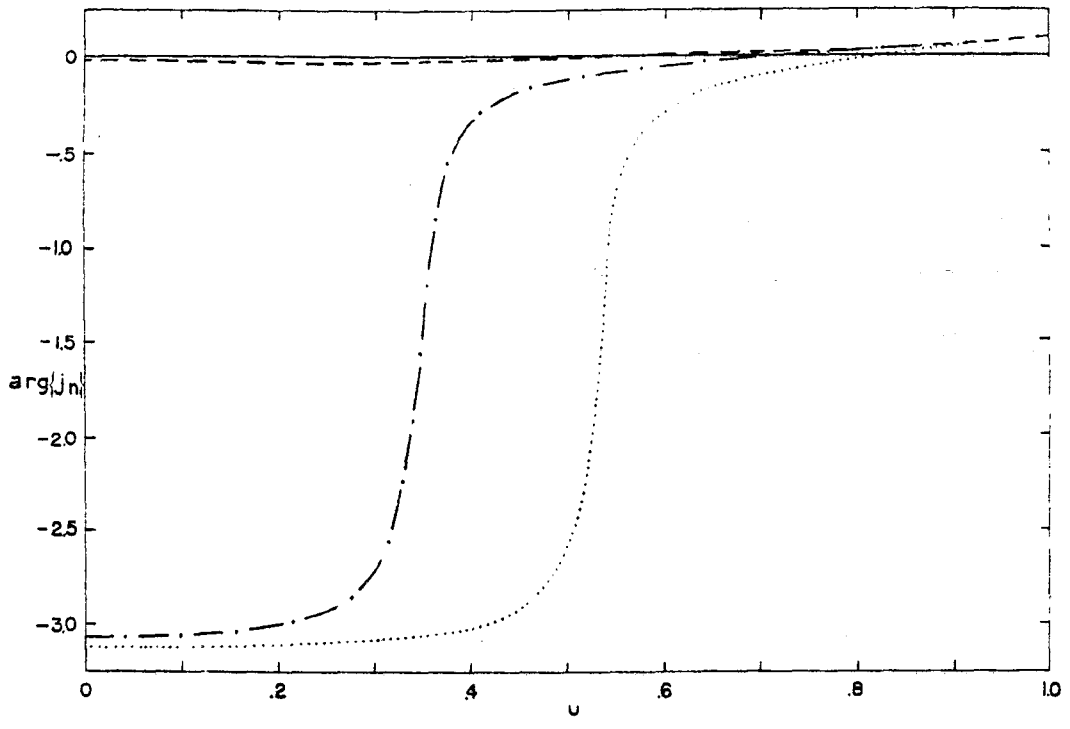
Figure 8. The phase variation of the current and charge distributions of natural modes of a solid cylinder where a/h = .05.

———— γh = -.194 + i1.334;   ------- γh = -.316 + i2.809
—·—·—·— γh = -.393 + i4.228;   ·······γh = -.507 + i5.823
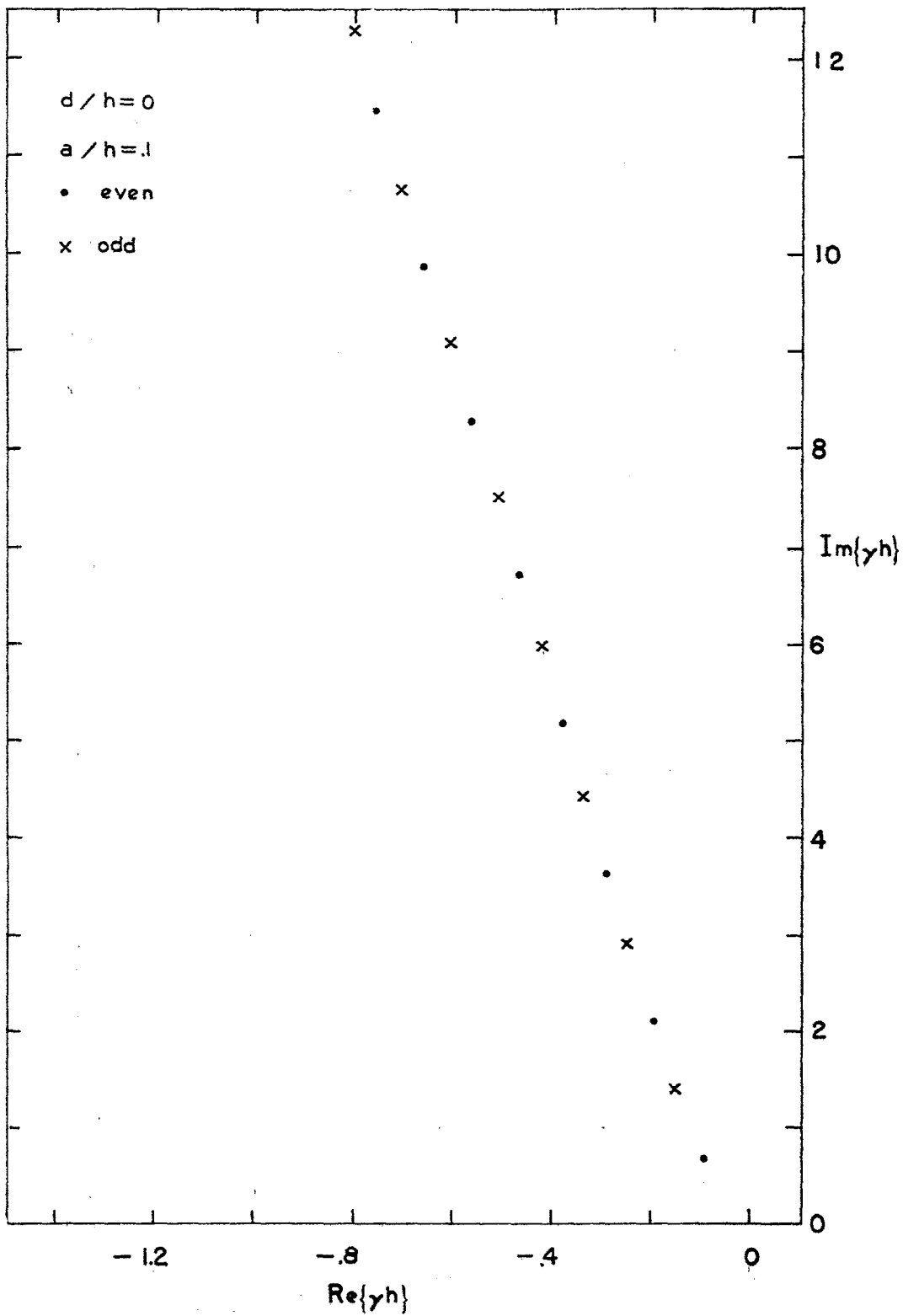
Figure 9. Natural frequencies of two, solid, collinear cylinders where d/h = 0 and a/h = .1.

24
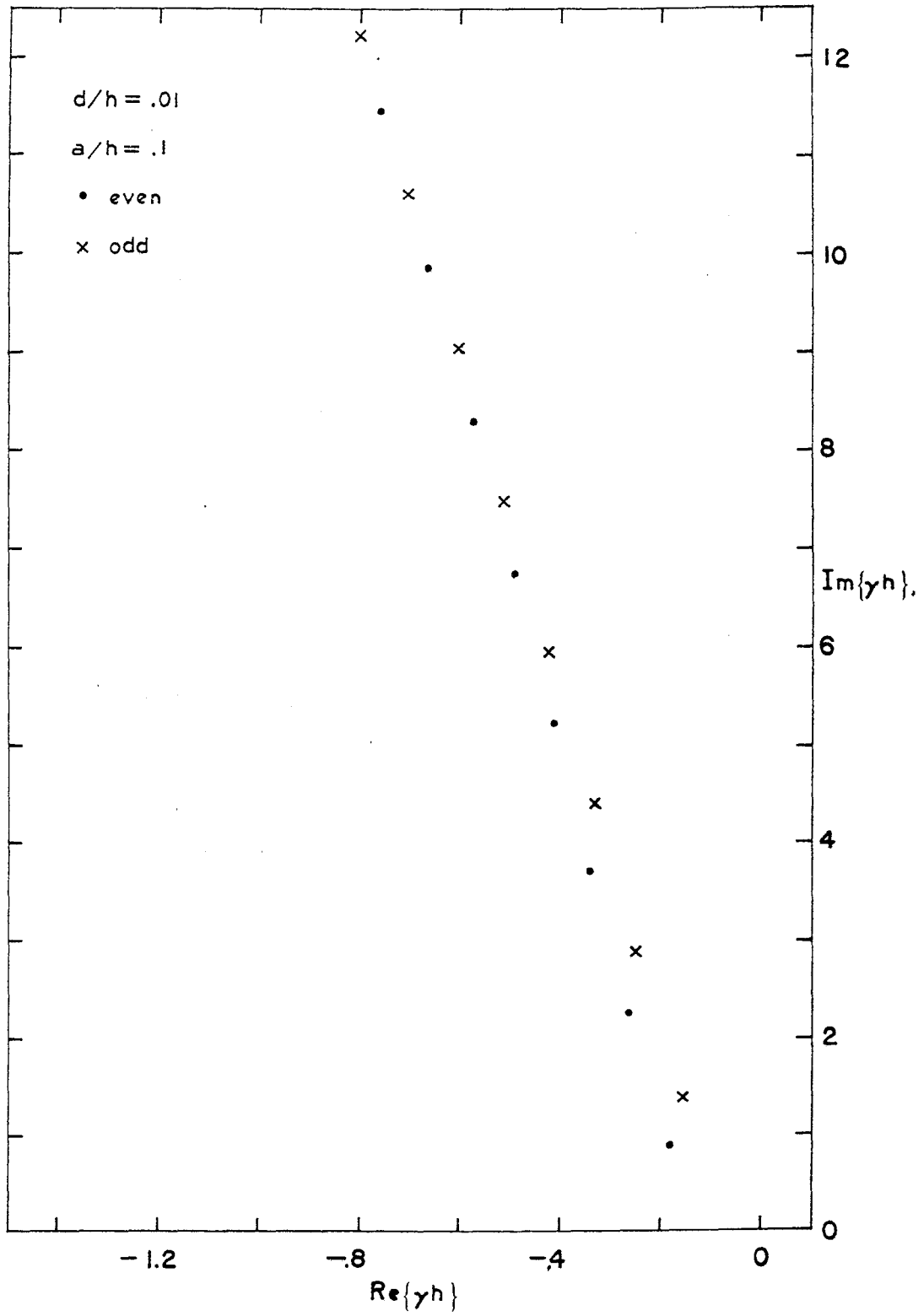
Figure 10. Natural frequencies of two solid, collinear cylinders where d/h = .01 and a/h = .1.
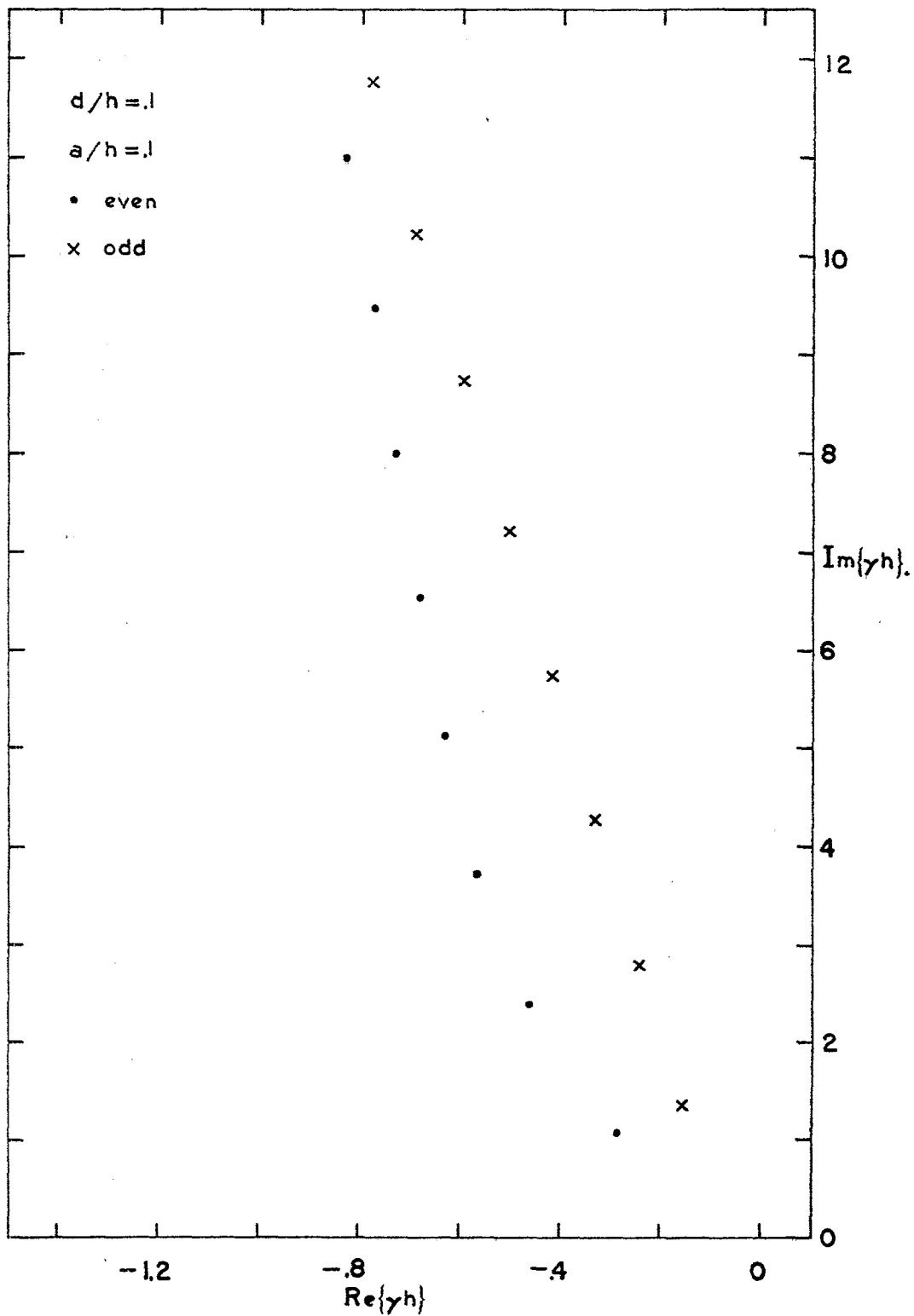
Figure 11.   Natural frequencies of two, solid, collinear cylinders where
d/h = .1 and a/h = .1.
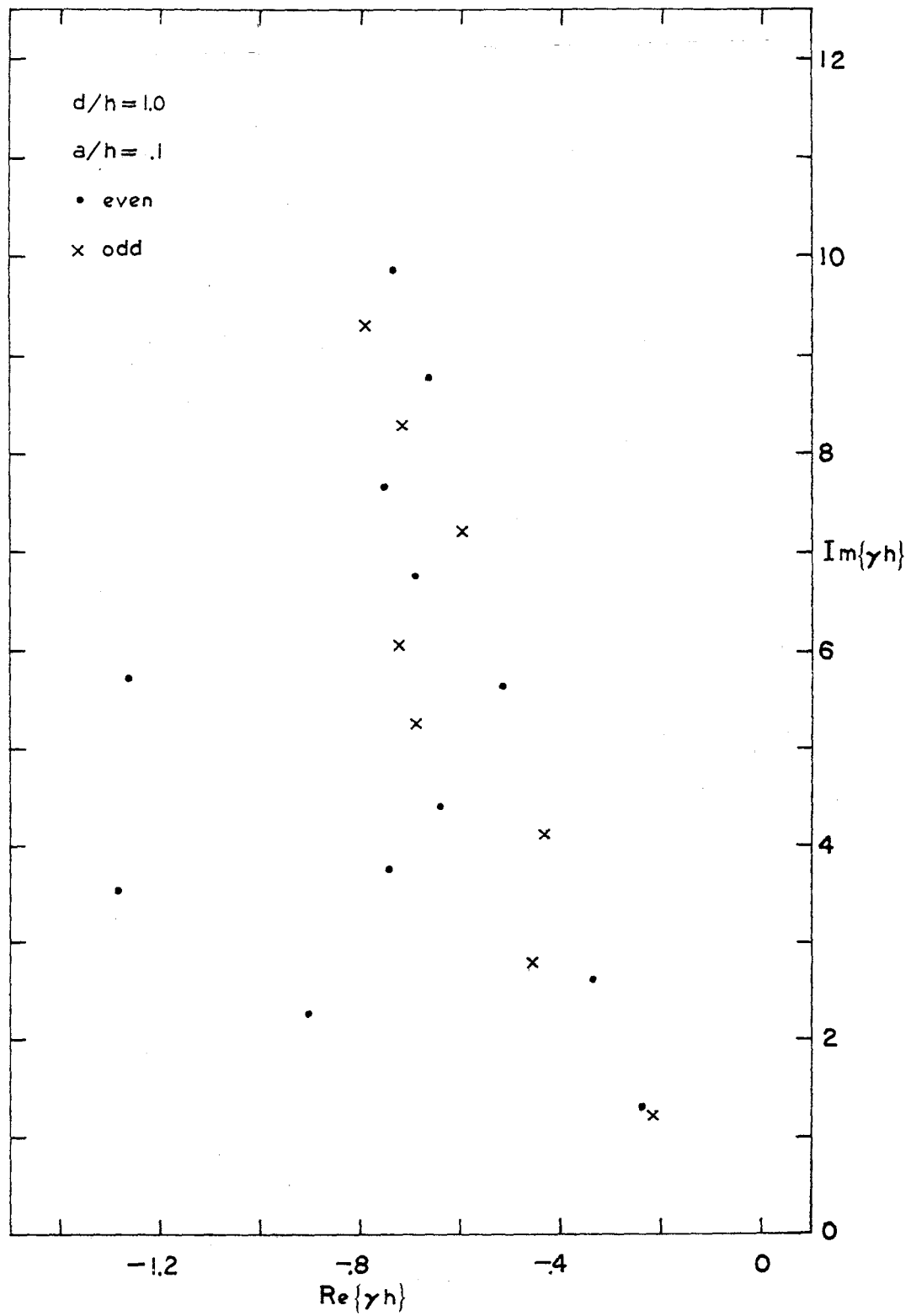
Figure 12. Natural frequencies of two solid, collinear cylinders where d/h = 1 and a/h = .1.

27
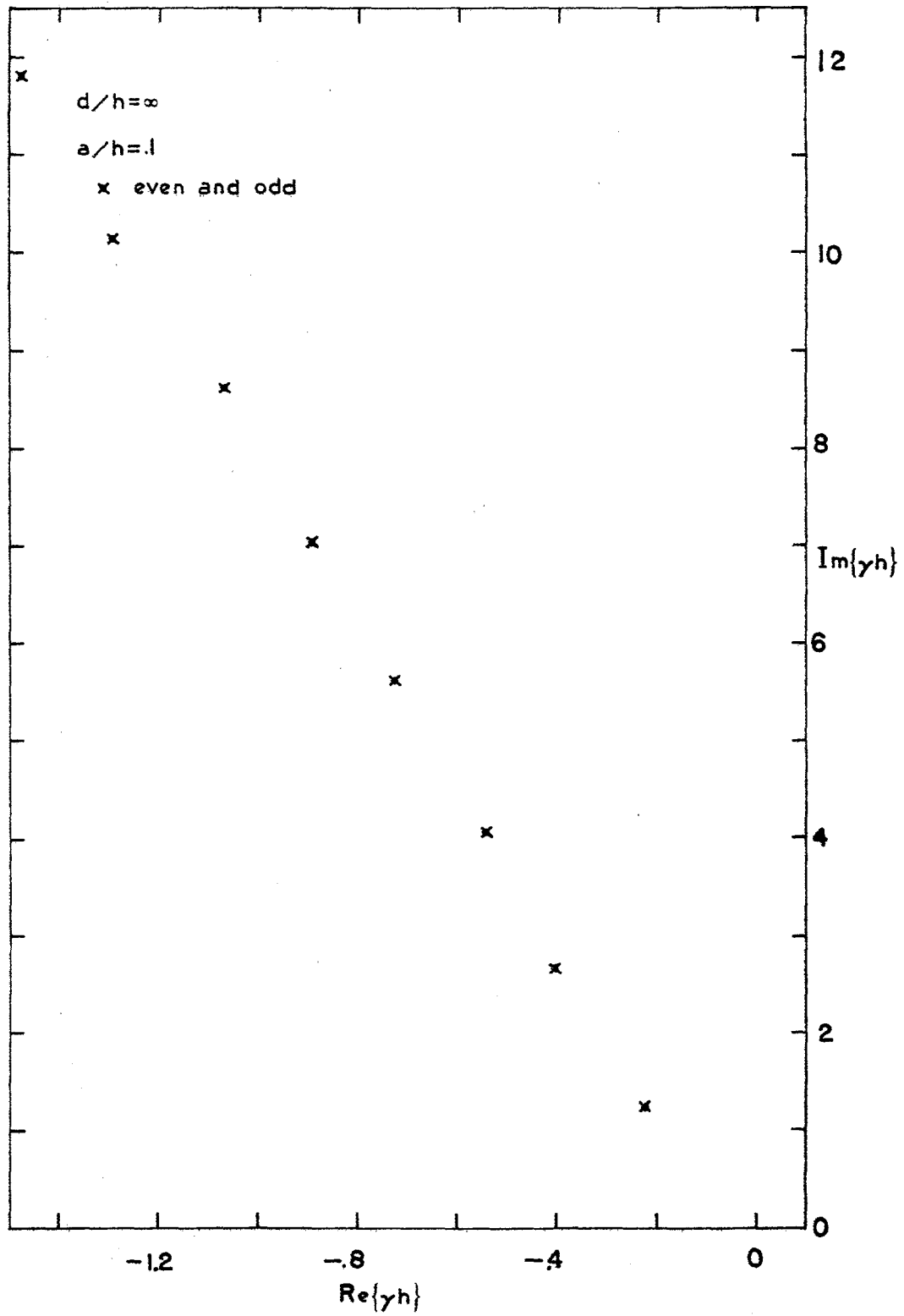
Figure 13. Natural frequencies of two, solid, collinear cylinders where $d/h \simeq \infty$ and $a/h = .1$ (one cylinder in free space).

28

Figure 14. Current and charge distributions of natural modes of two, solid, collinear cylinders where $d/h = 0$ and $a/h = .1$.

The legend for the figure reads:
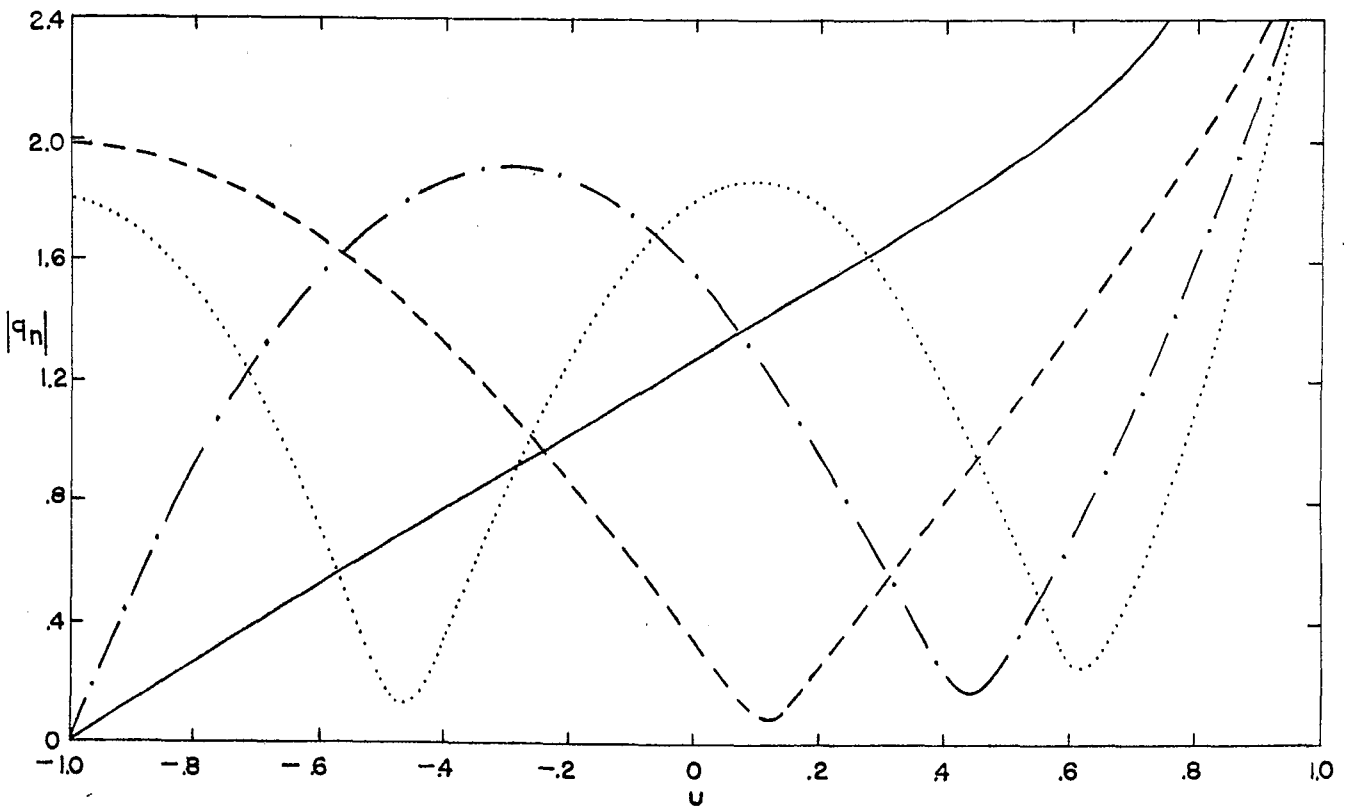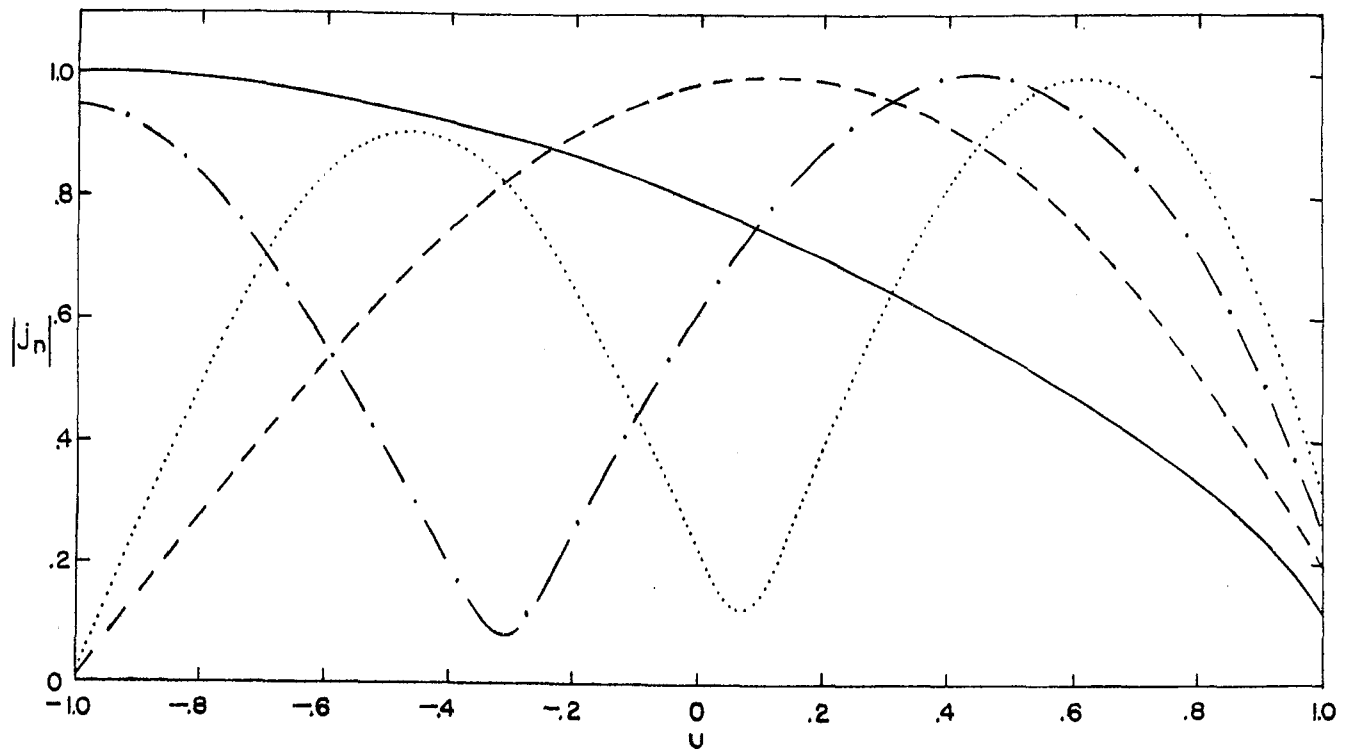
$\gamma h = -.097 + i\ .667$; $\gamma h = -.158 + i1.405$

$\gamma h = -.196 + i2.117$; $\gamma h = -.254 + i2.912$
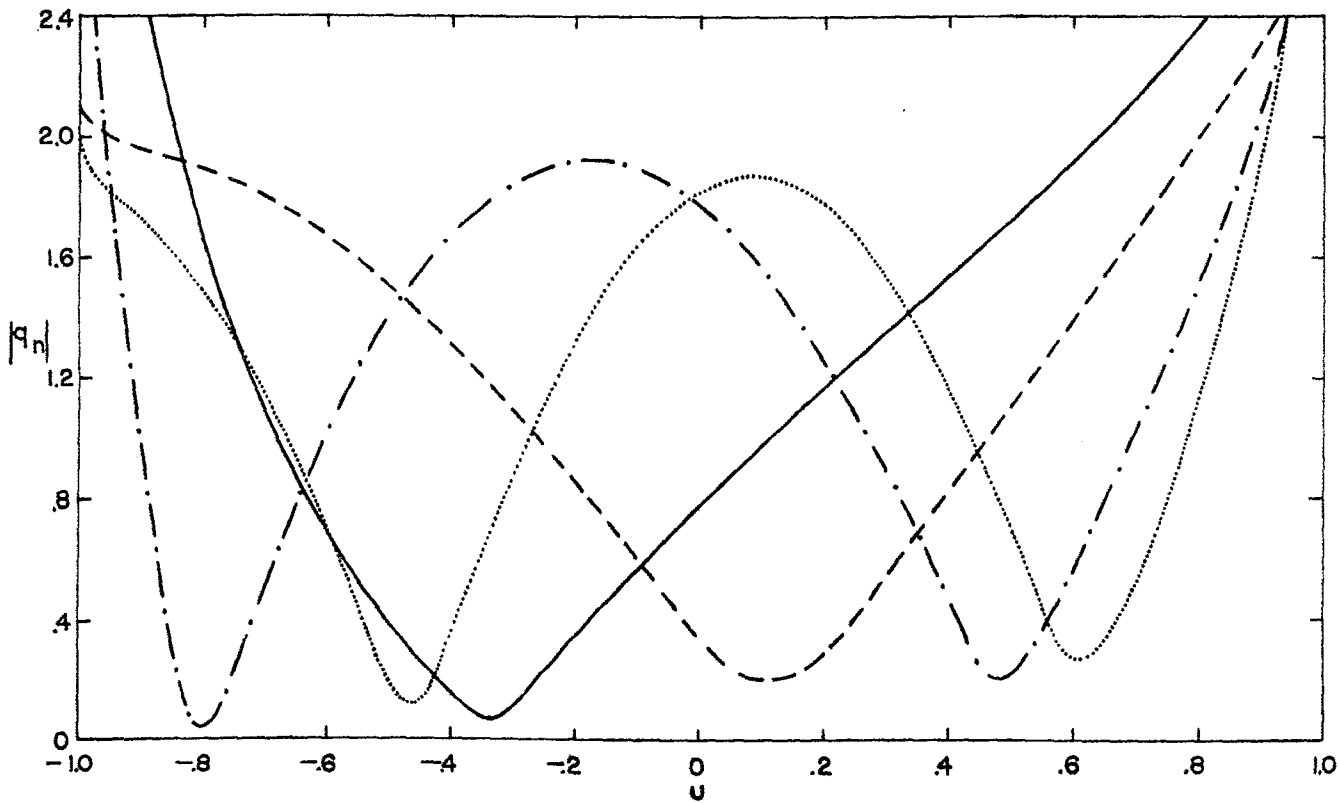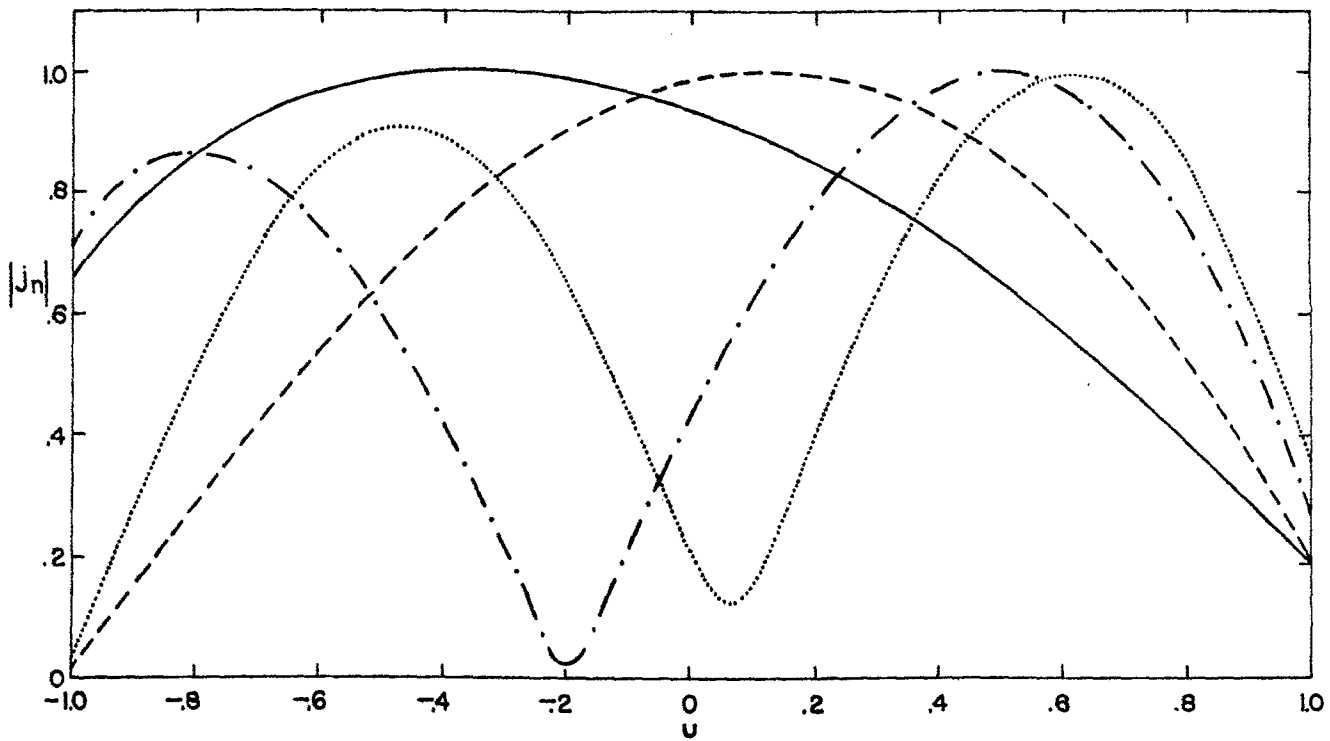
Figure 15. Current and charge distributions of natural modes of two, solid, collinear cylinders where d/h = .01 and a/h = .1.
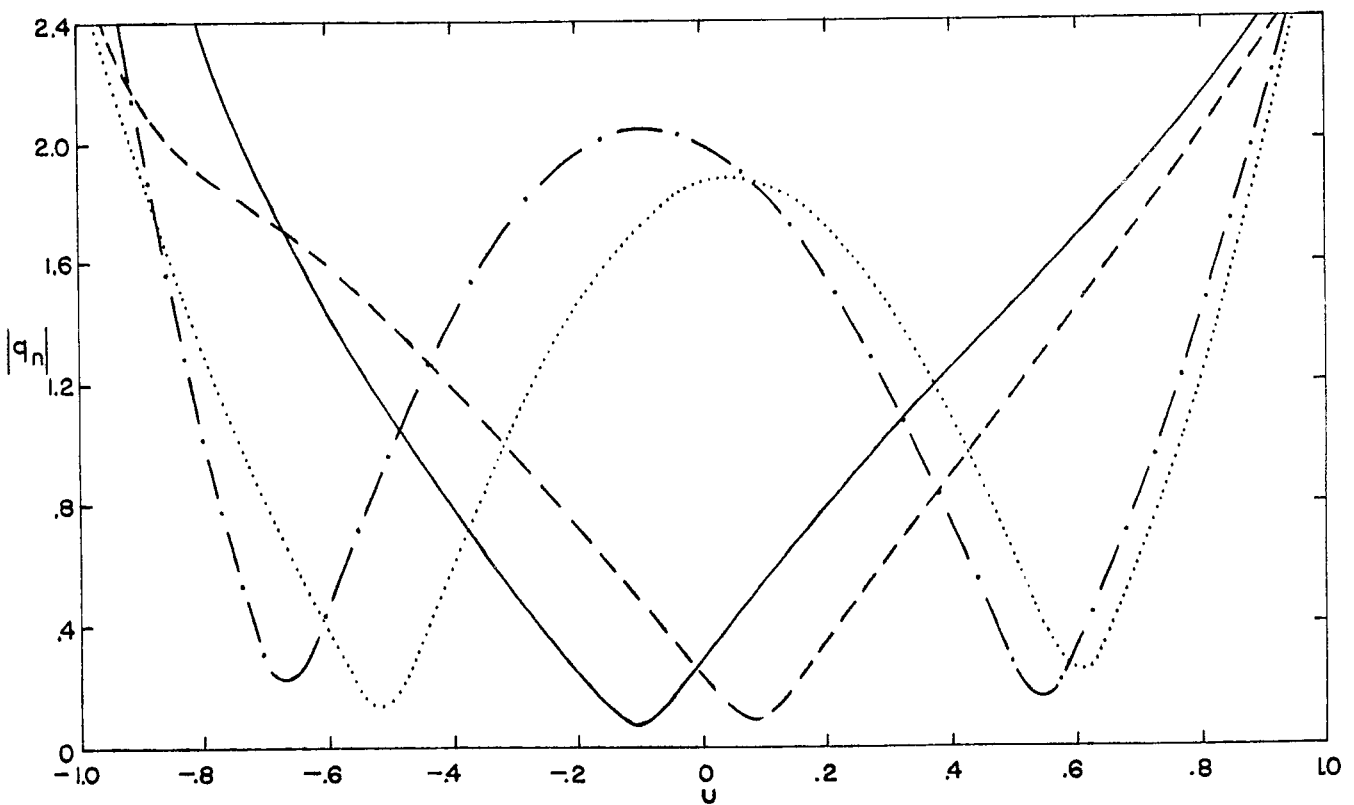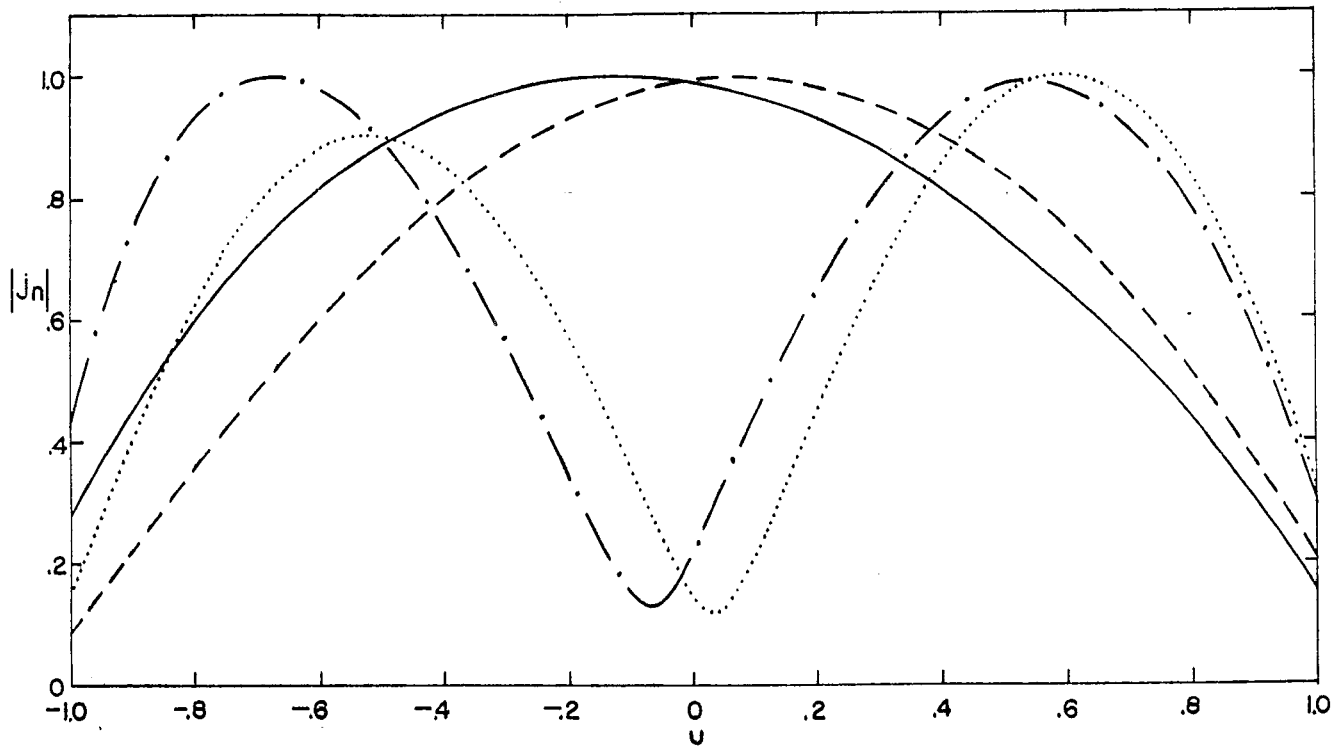
Figure 16. Current and charge distributions of natural modes of two, solid, collinear cylinders where d/h = .1 and a/h = .1.
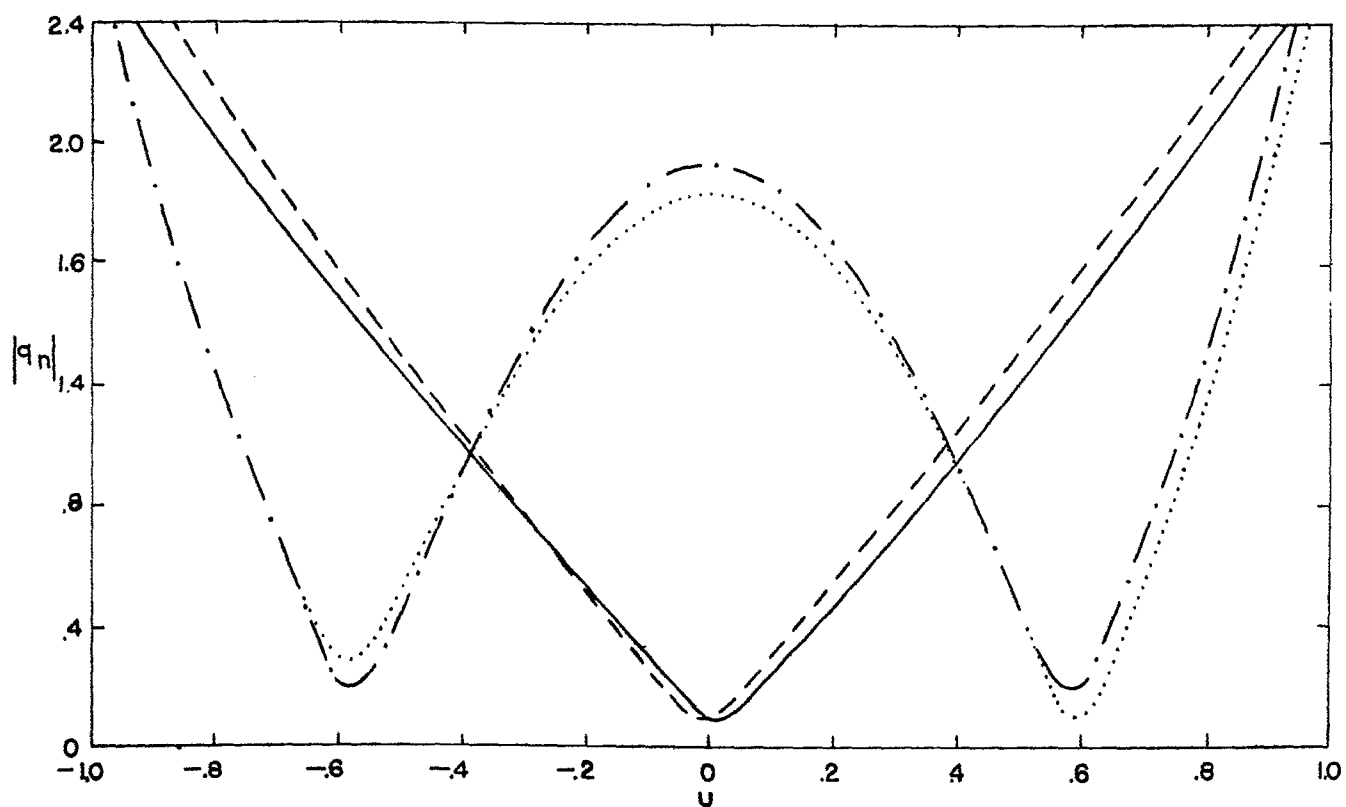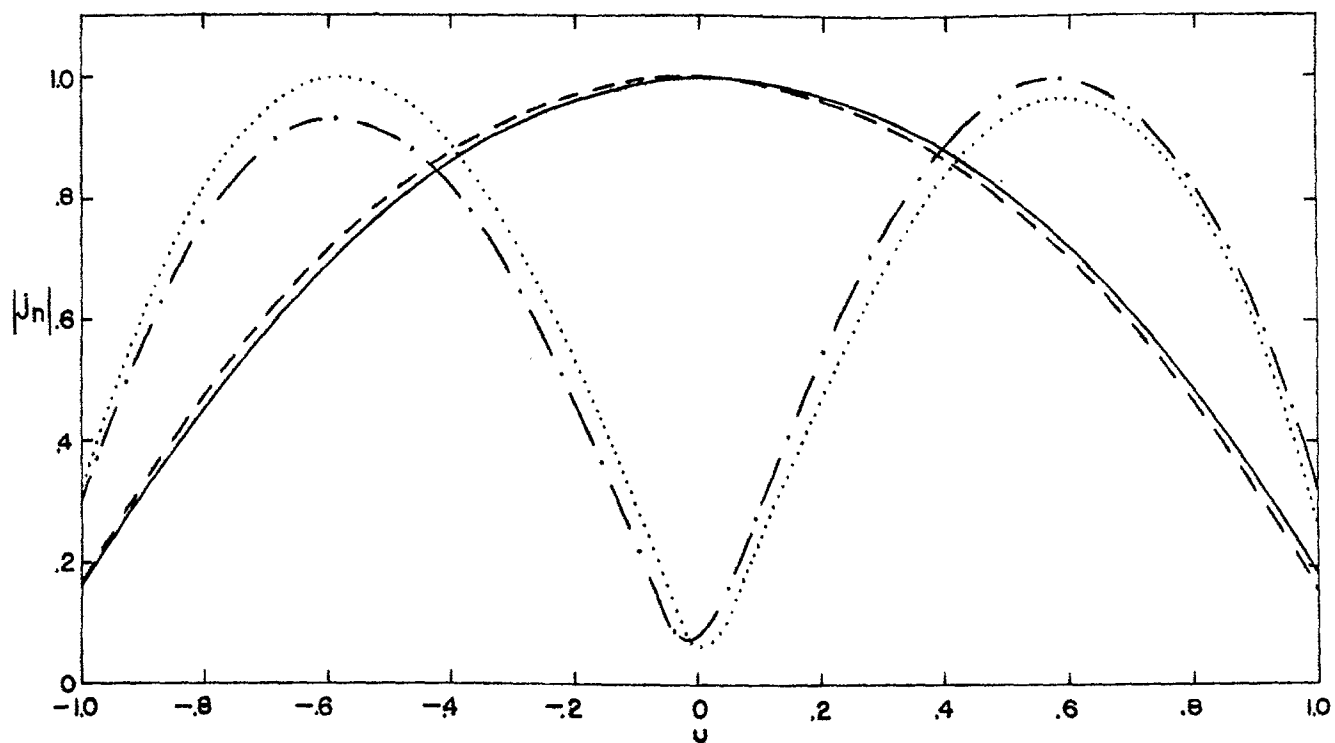
Figure 17. Current and charge distributions of natural modes of two, solid, collinear cylinders where d/h = 1 and a/h = .1.

Figure 18. Current and charge distributions of natural modes of two, solid, collinear cylinders where $d/h = \infty$ and $a/h = .1$ (one cylinder in free space).

The legend within the figure:
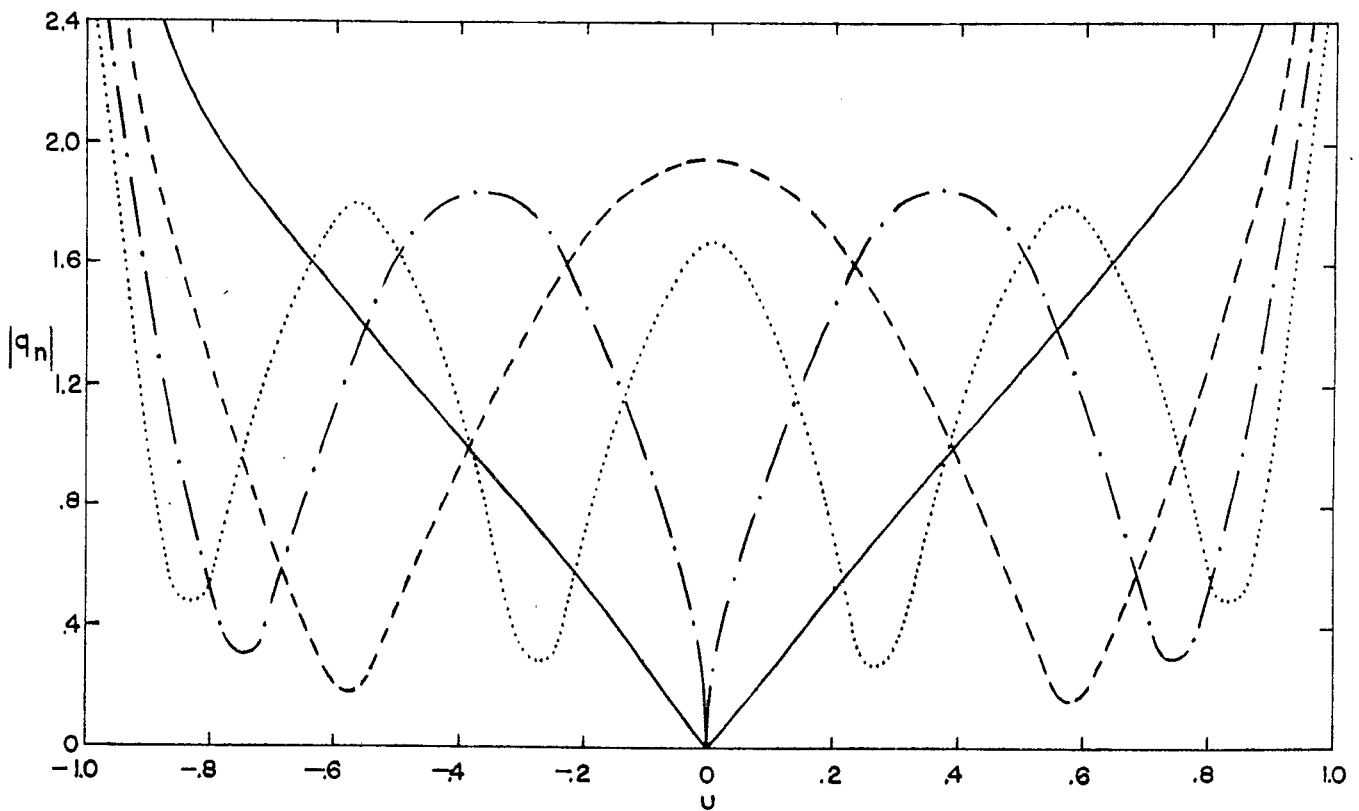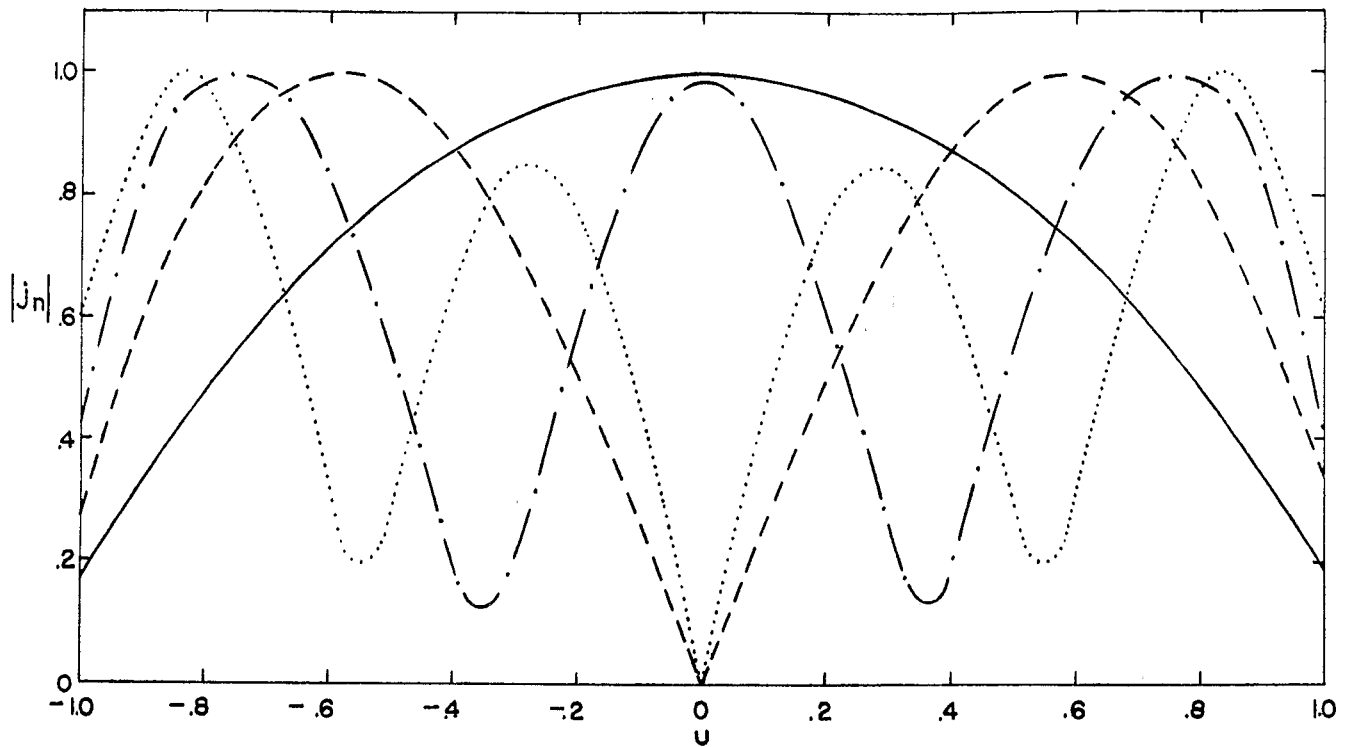
$\gamma h = -.222 + i1.253$; $\gamma h = -.409 + i2.688$
$\gamma h = -.549 + i4.088$; $\gamma h = -.727 + i5.635$
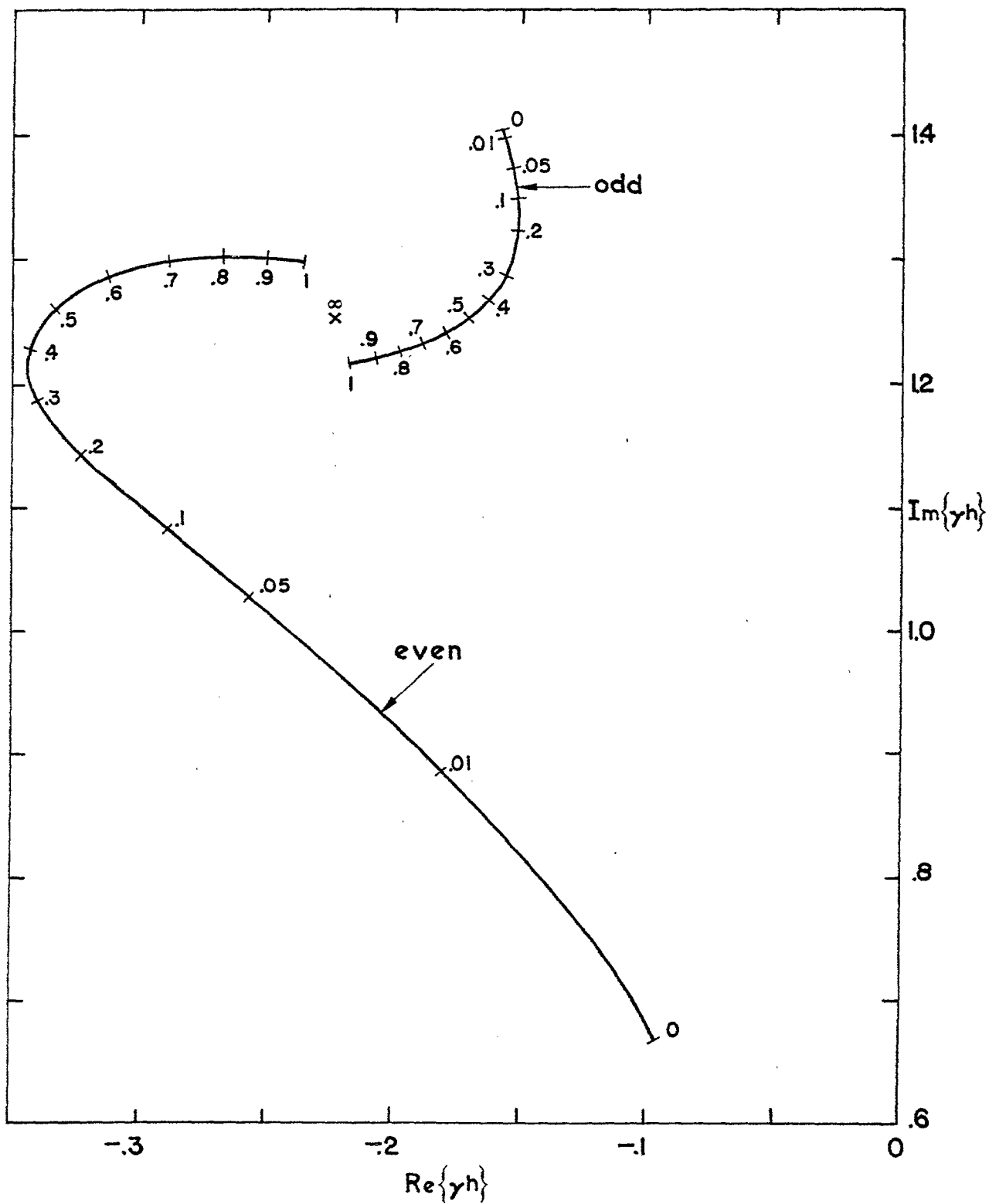
Figure 19. Loci of the first natural frequency when 0 < d/h < 1.

34
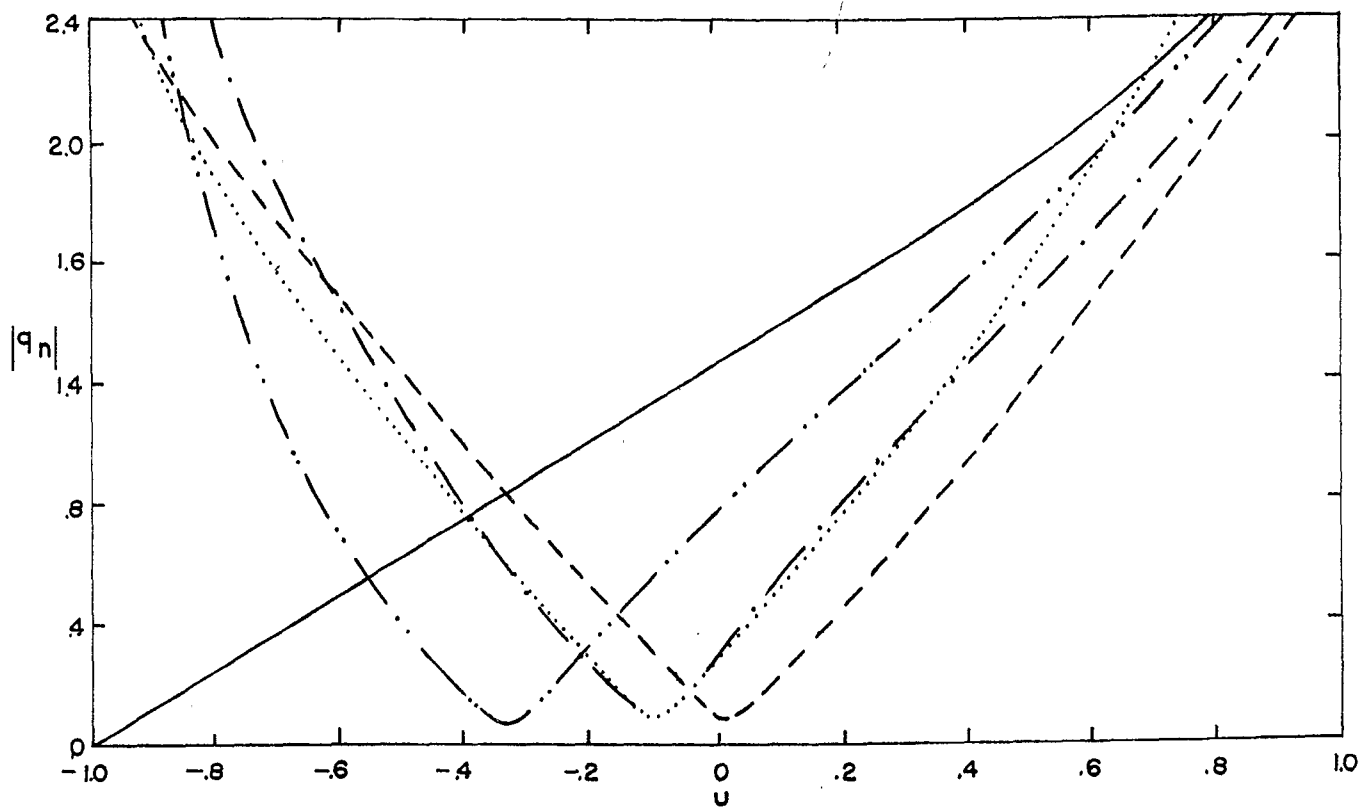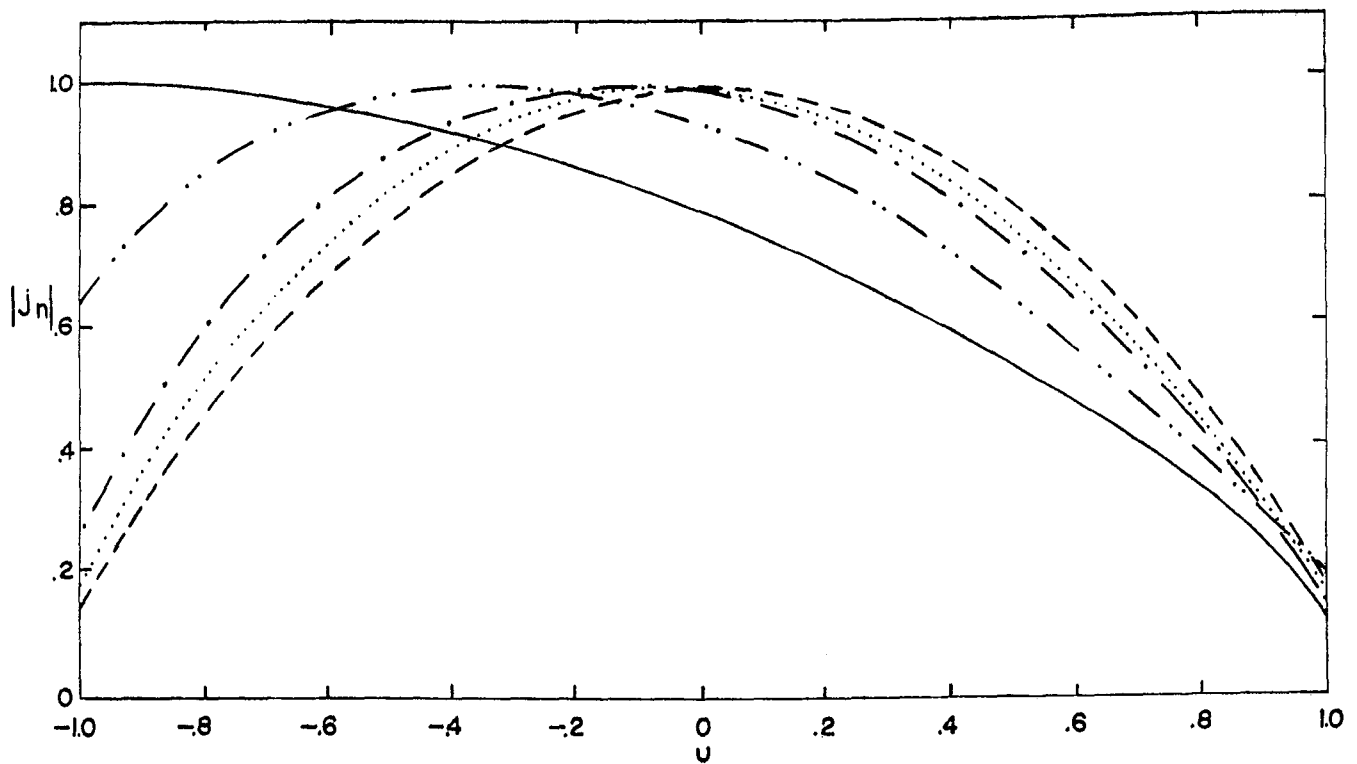
Figure 20. Current and charge distributions of the first even natural mode
for a/h = .1 and different values of d/h.
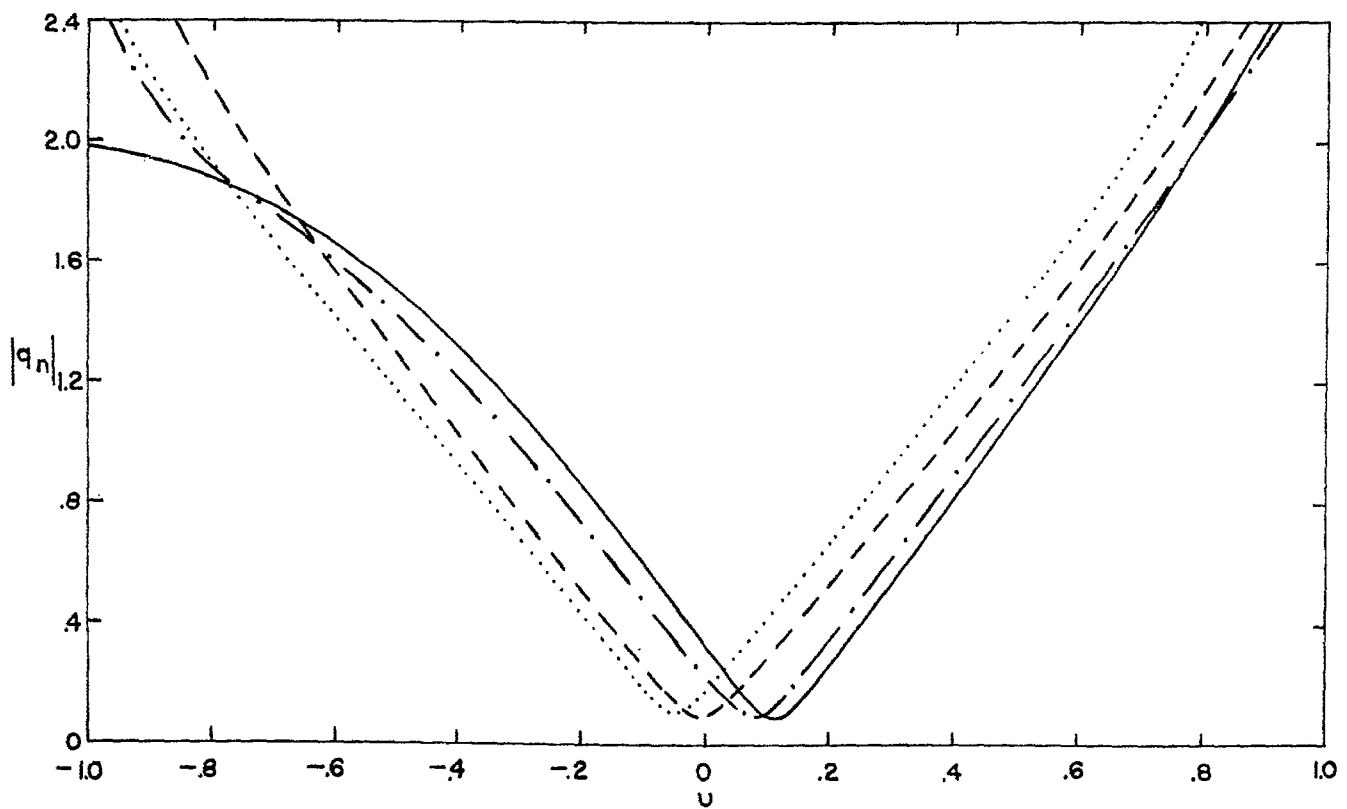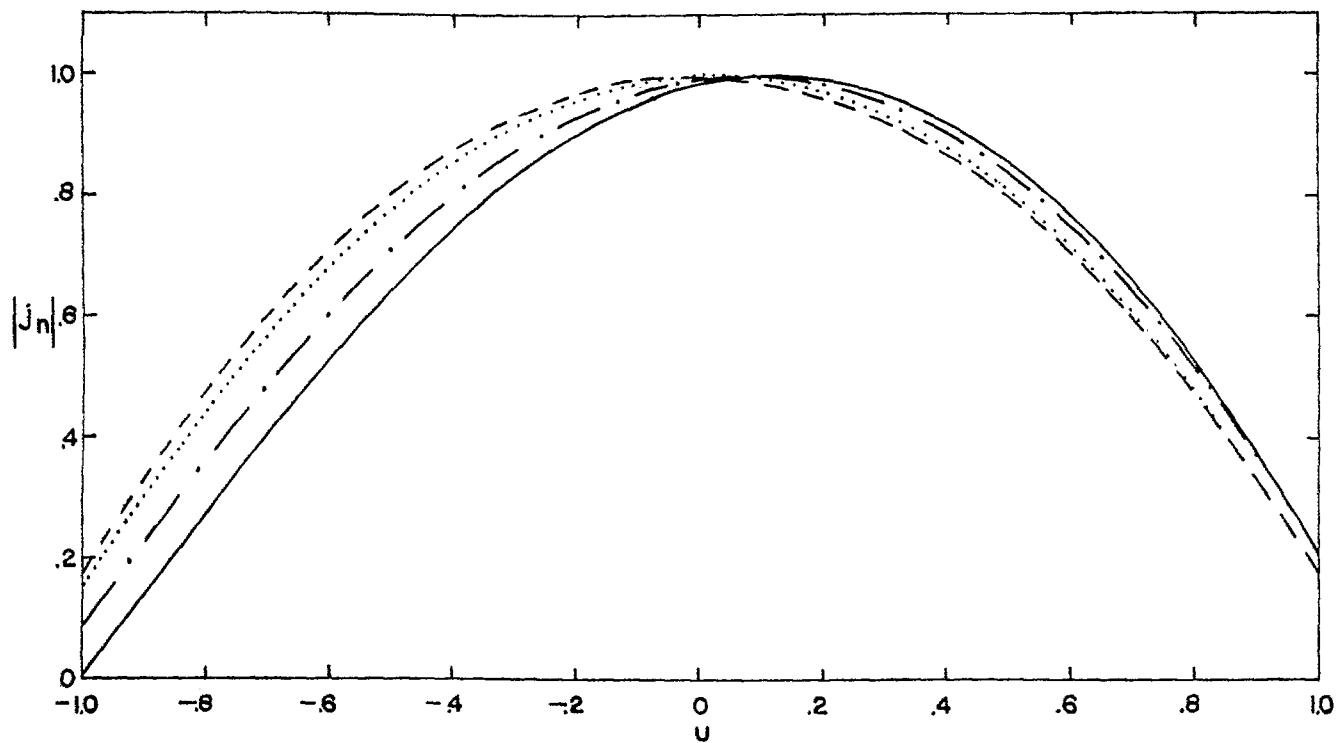
Figure 21.   Current and charge distributions of the first odd natural mode
             for a/h = .1 and different values of d/h.
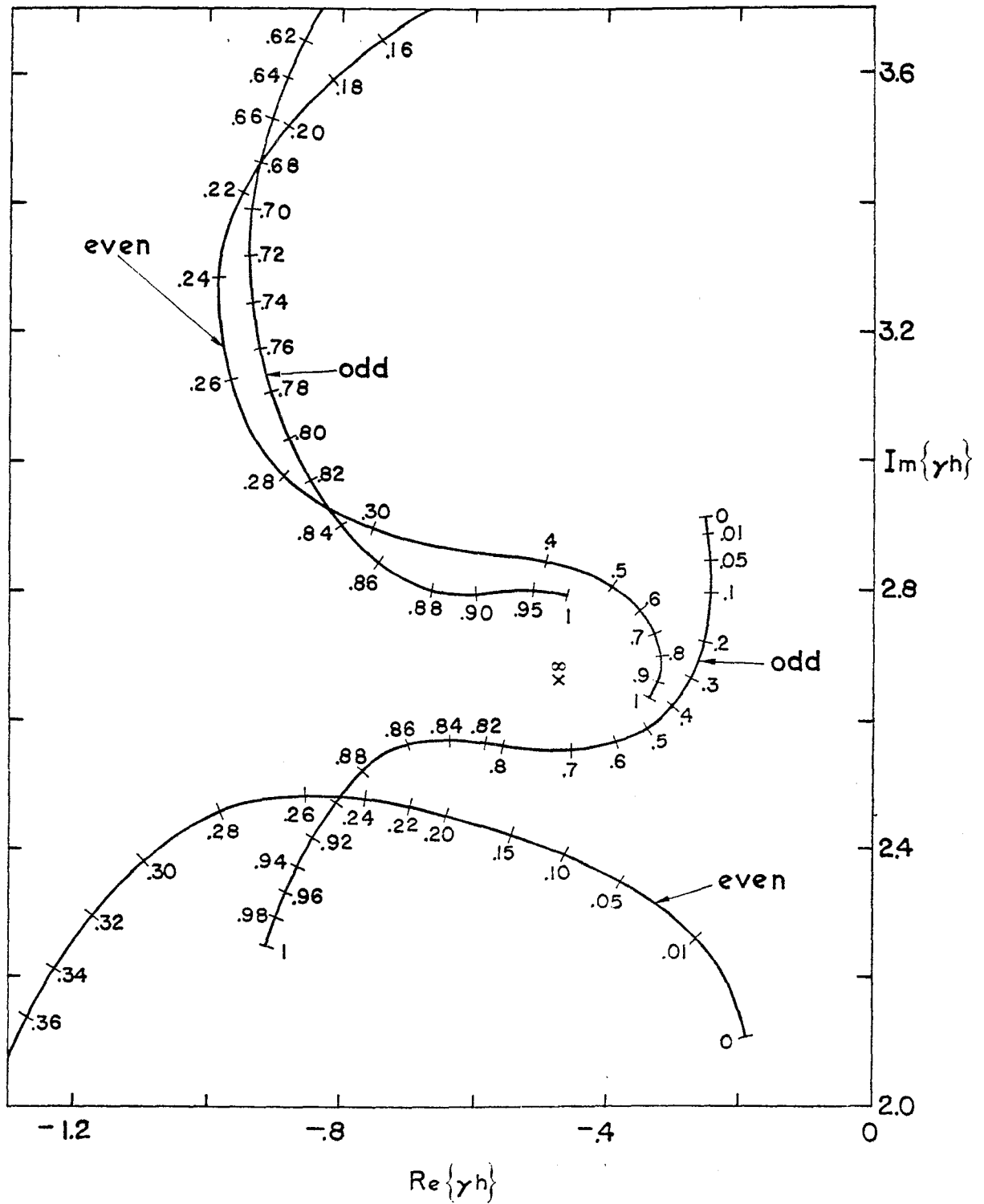
Figure 22. Loci of the "second" natural frequency when 0 < d/h < 1.
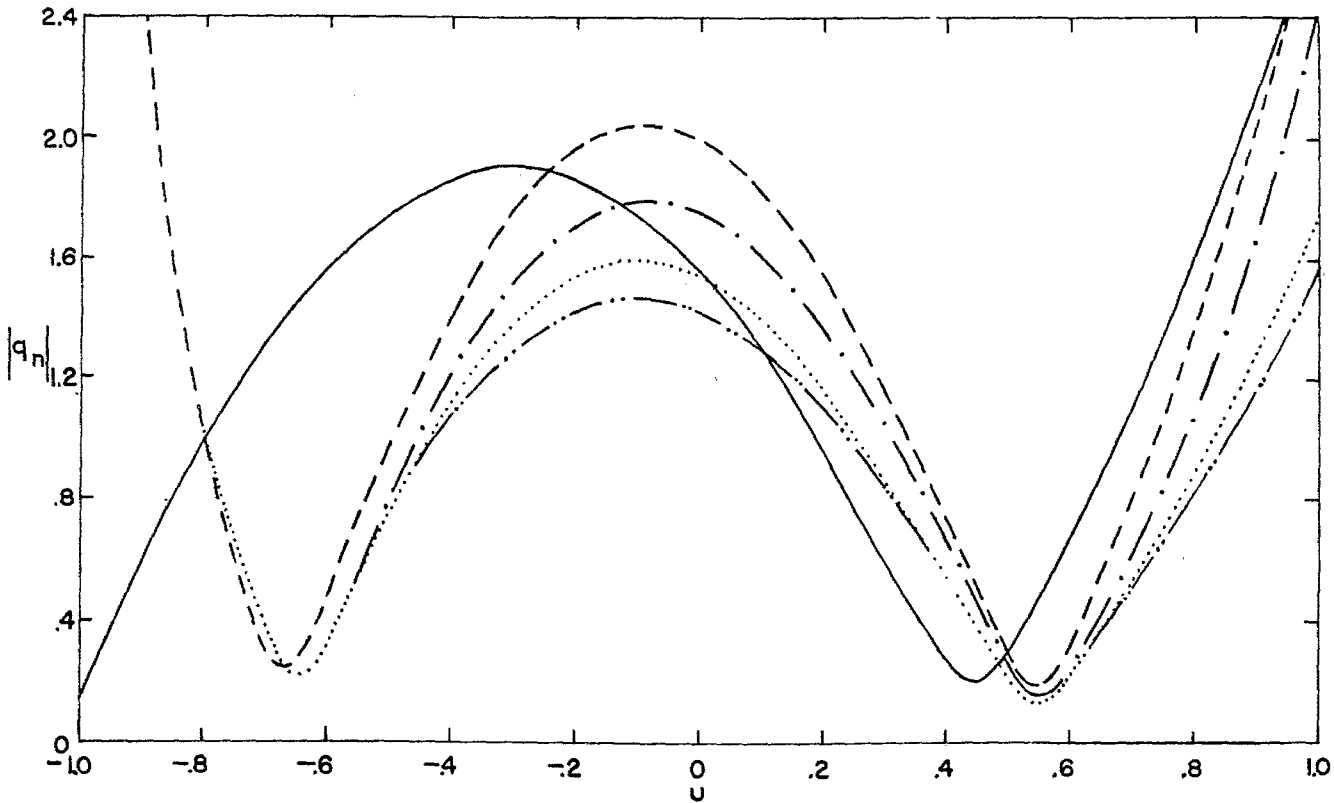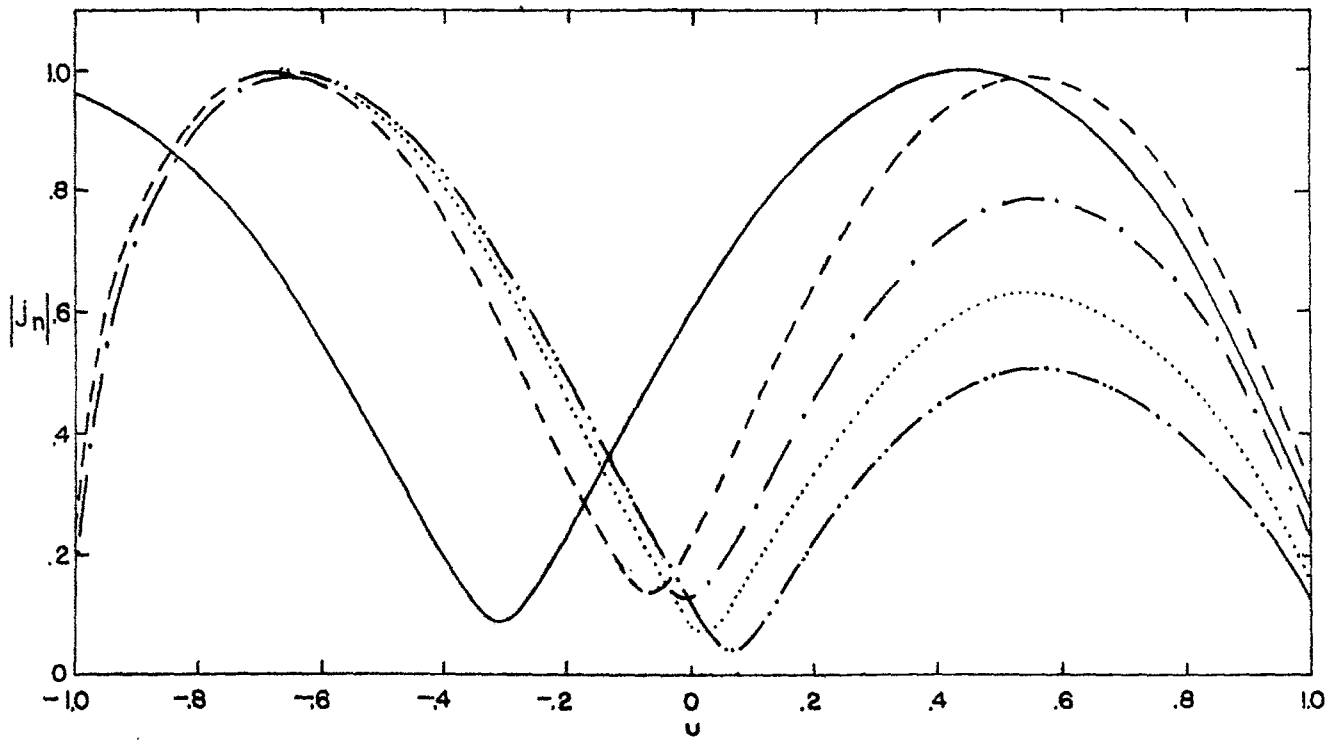
Figure 23. Current and charge distributions of the "second" even natural mode for a/h = .1 and different values of d/h.

The legend in the figure:

——————d/h = 0, γh = − .196 + i2.114;　————————d/h = .1,　γh = −.463 + i2.388

—·——·—·—d/h = .2, γh = − .648 + i2.436;　·······d/h = .26,　γh = −.850 + i2.481

—·—··—··—d/h = .3, γh = −1.094 + i2.379;
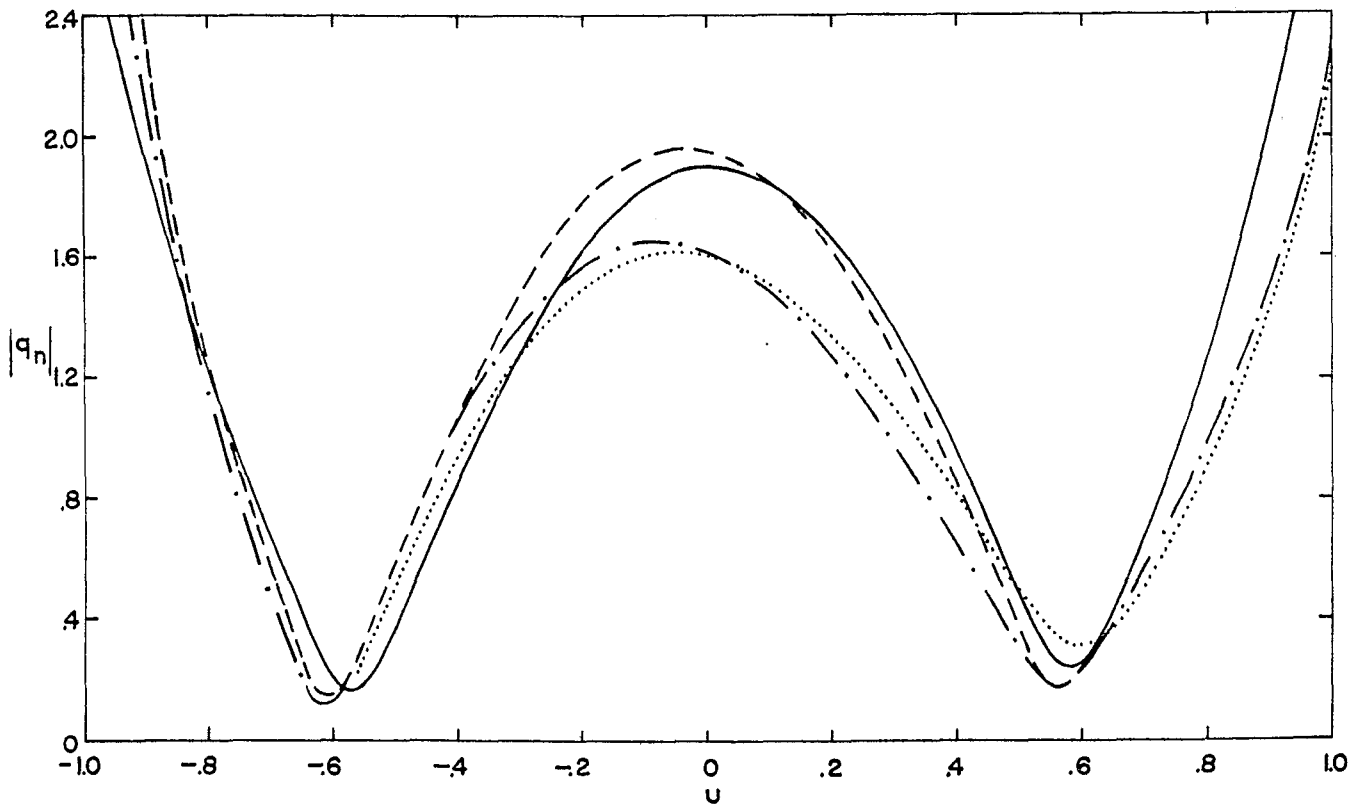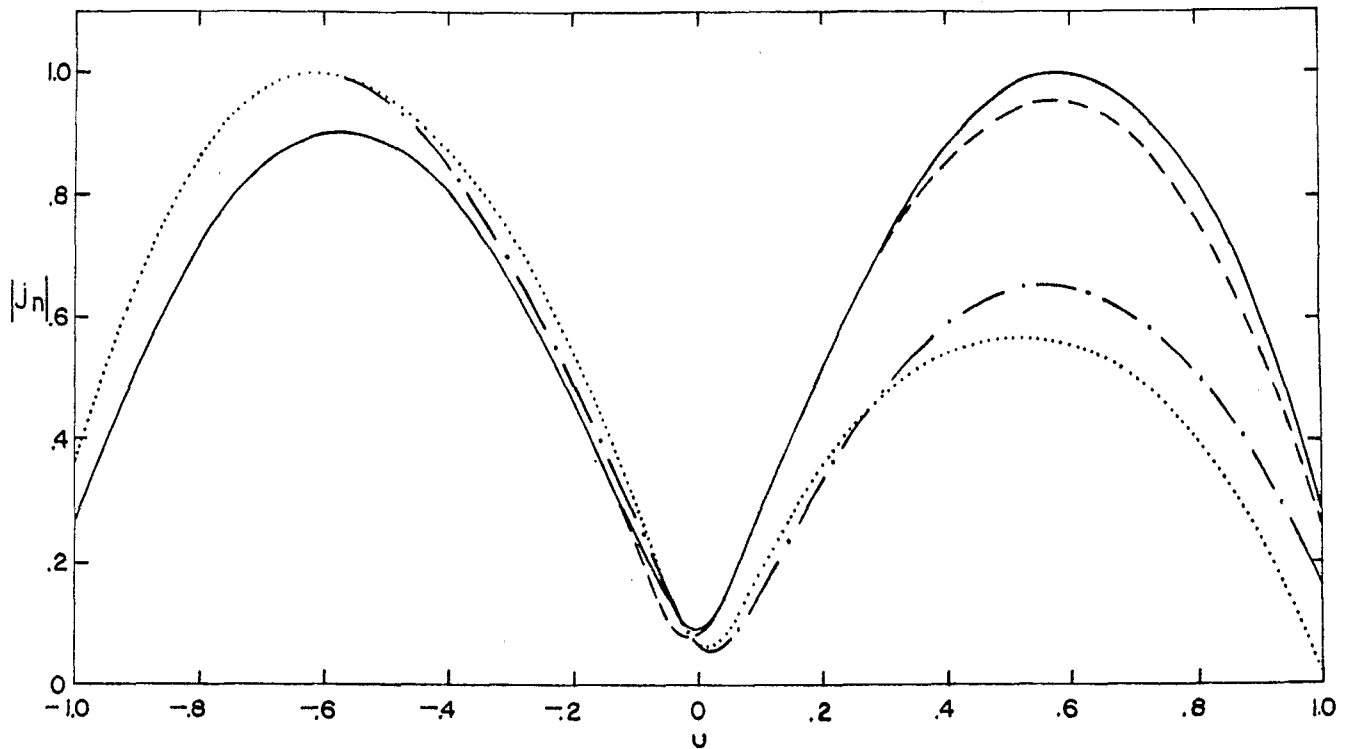
Figure 24. Current and charge distributions of the "second" odd natural mode for a/h = .1 and different values of d/h.

―――――d/h = .3, γh = -.274 + i2.667;   ―――――d/h = .7, γh = -.453 + i2.555
―・―・―d/h = .9, γh = -.809 + i2.469;   ・・・・・・d/h = 1, γh = -.805 + i2.153
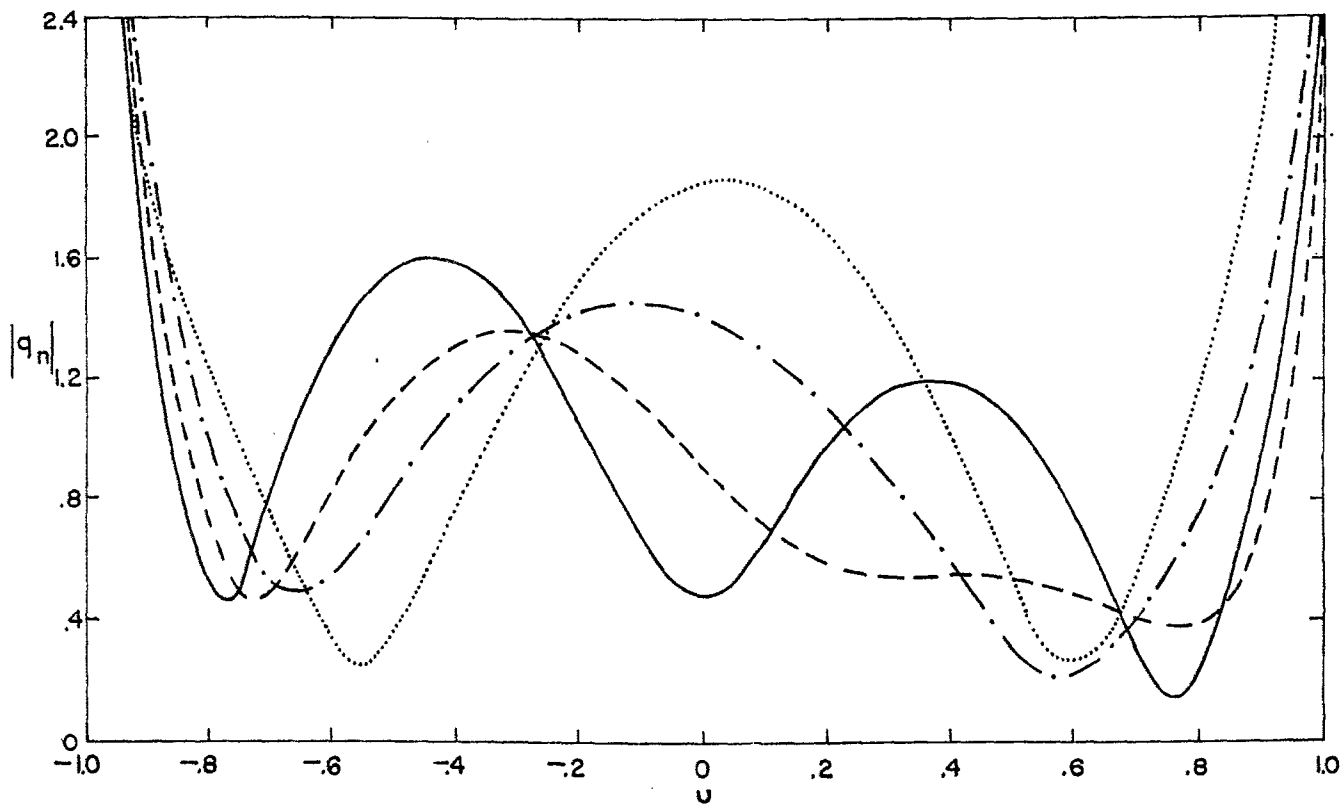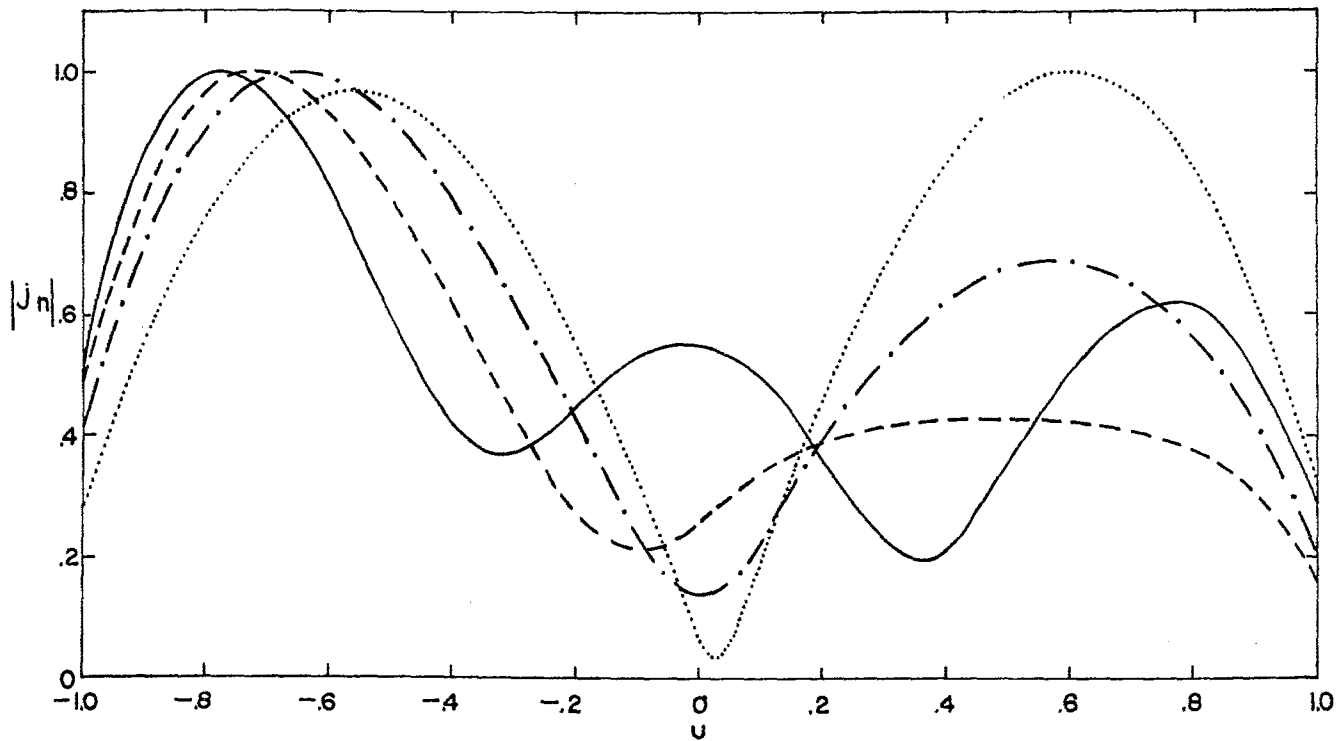
------ d/h = .2, γh = −.881 + i3.519; ------- d/h = .26, γh = −.968 + i3.129

—·—·— d/h = .3, γh = −.754 + i2.891; ·······d/h = .5, γh = −.399 + i2.809

Figure 25. Current and charge distributions of the "second" even natural mode for a/h = .1 and different values of d/h.

Figure 26. Current and charge distributions of the "second" odd natural mode
for a/h = .1 and different values of d/h.
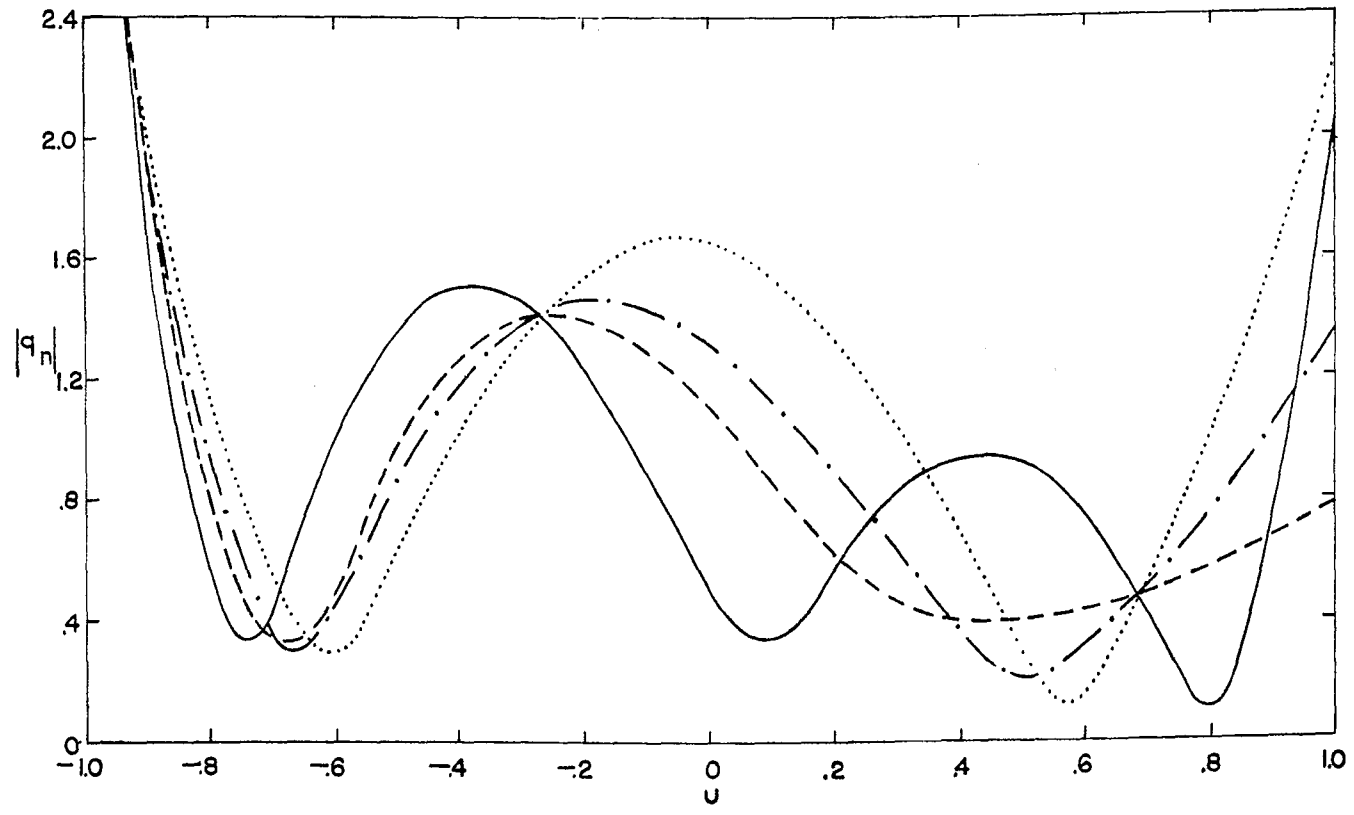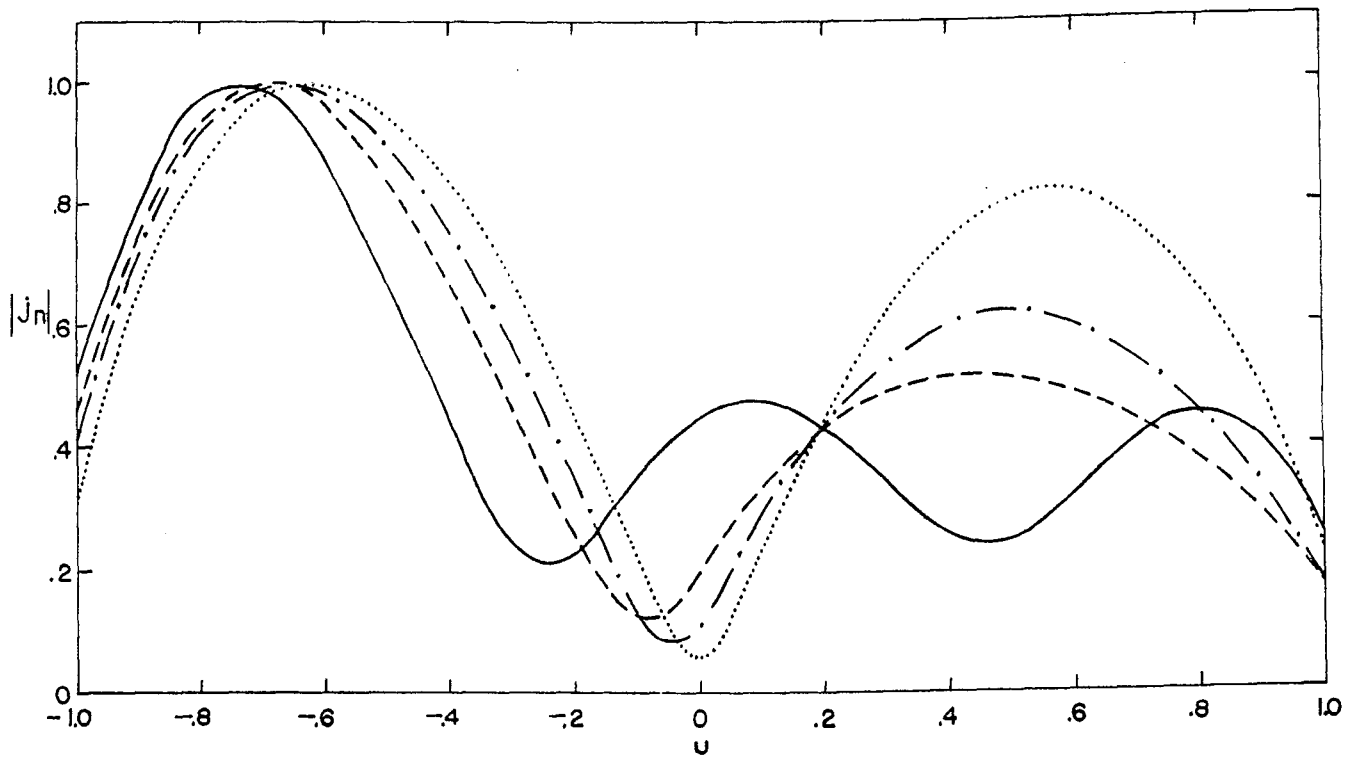
——————d/h = .7,   γh = −.936 + i3.389;   ———————d/h = .8, γh = −.876 + i3.037
—·—·—·d/h = .84, γh = −.803 + i2.906;   ·······d/h = .9, γh = −.598 + i2.795
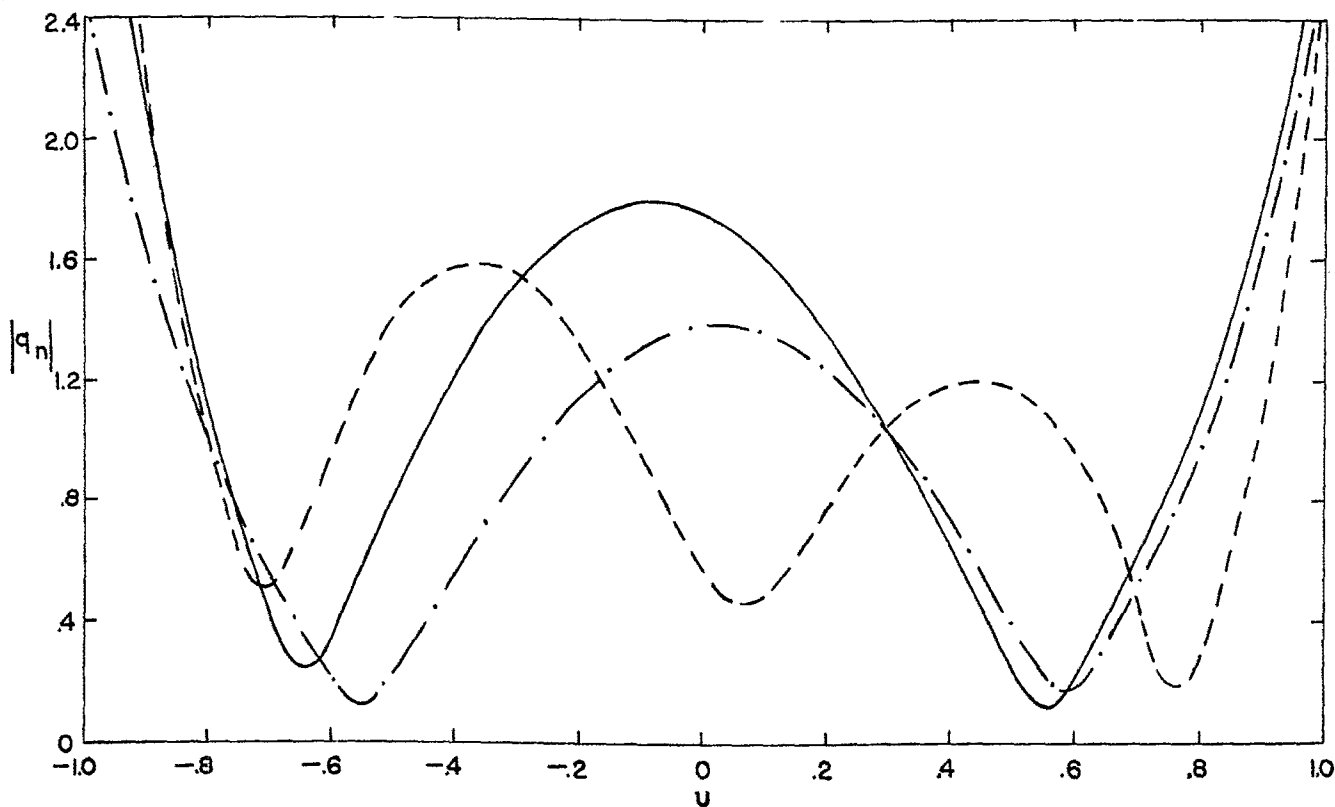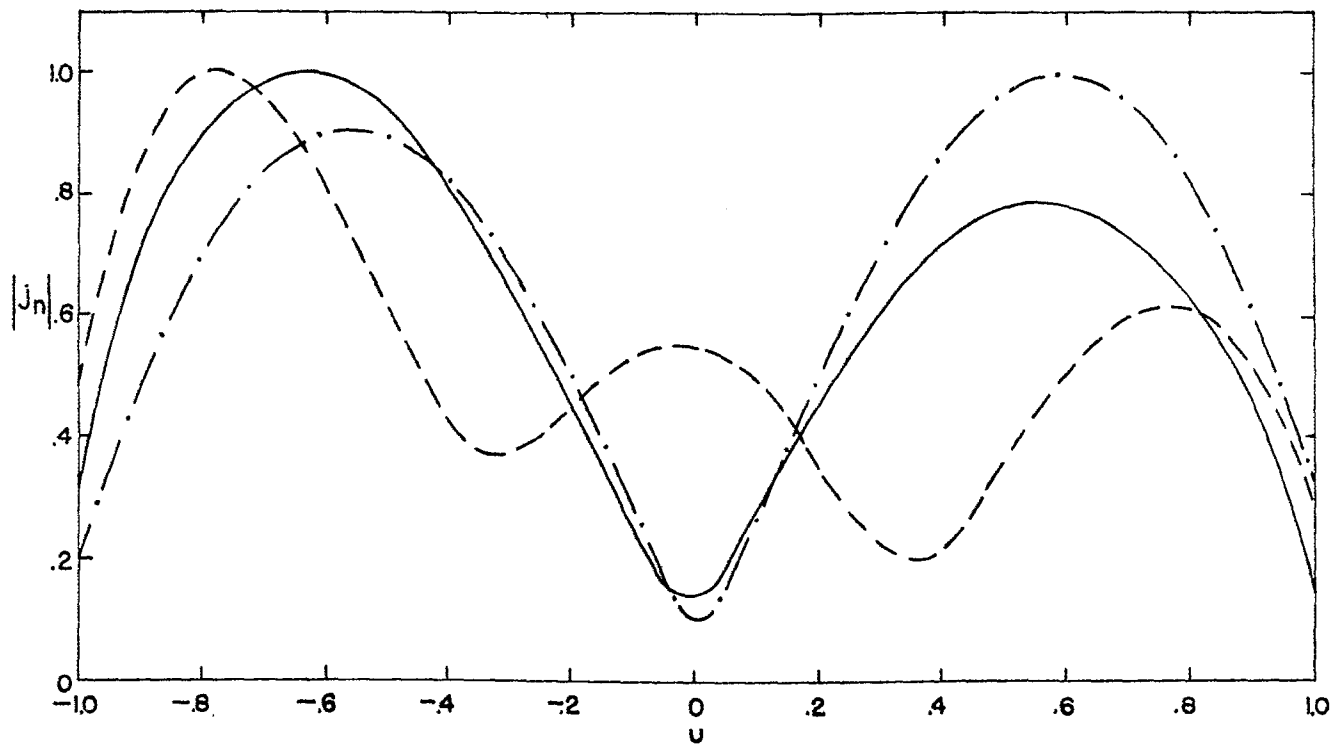
Figure 27. Current and charge distributions of the "second" natural mode for $a/h = .1$ and $d/h = .2$.

The legend:
———$\gamma h = -.648 + i2.436$;   ———————$\gamma h = -.881 + i3.519$
—·—·—·—$\gamma h = -.255 + i2.722$

Figure 28. Current and charge distributions of the "second" natural mode for $a/h = .1$ and $d/h = .3$.

Legend:
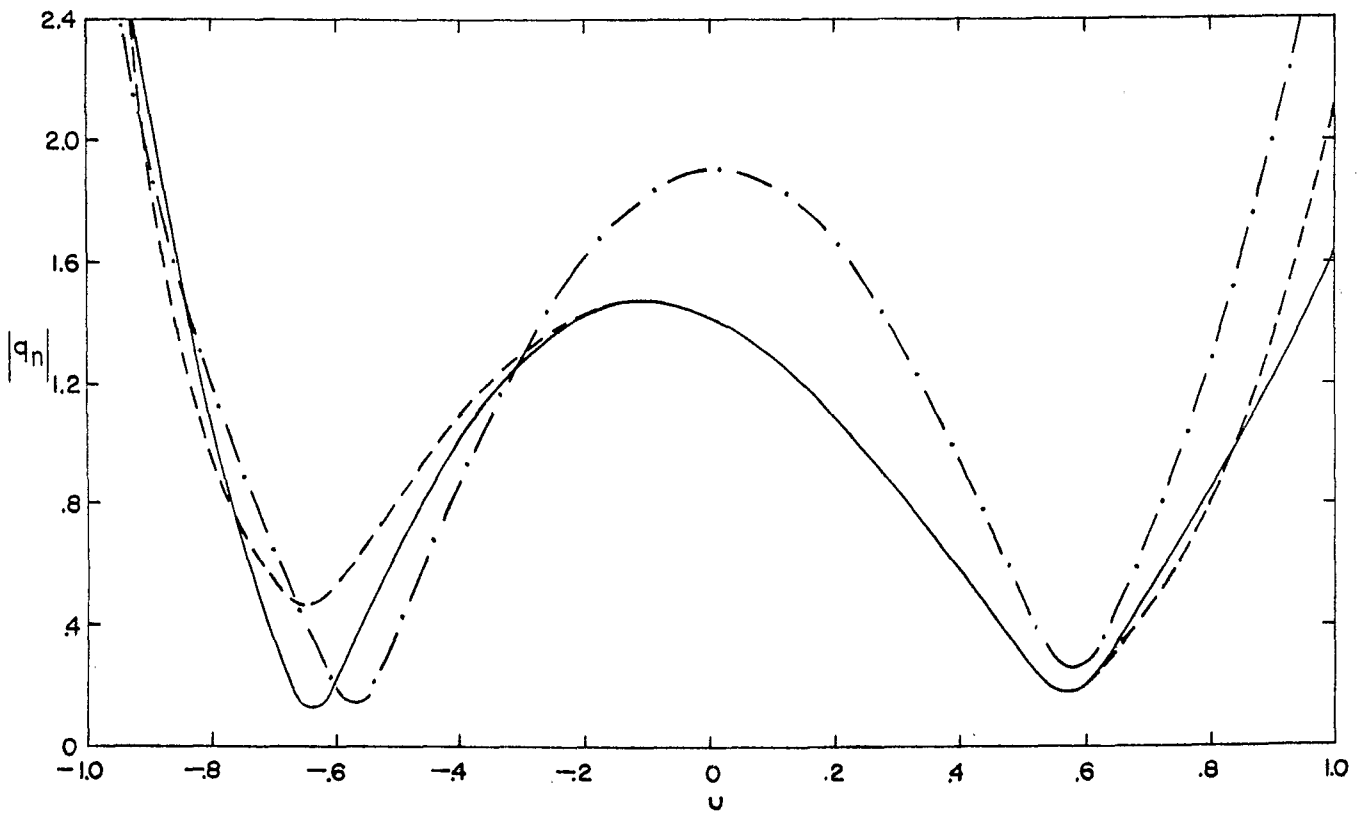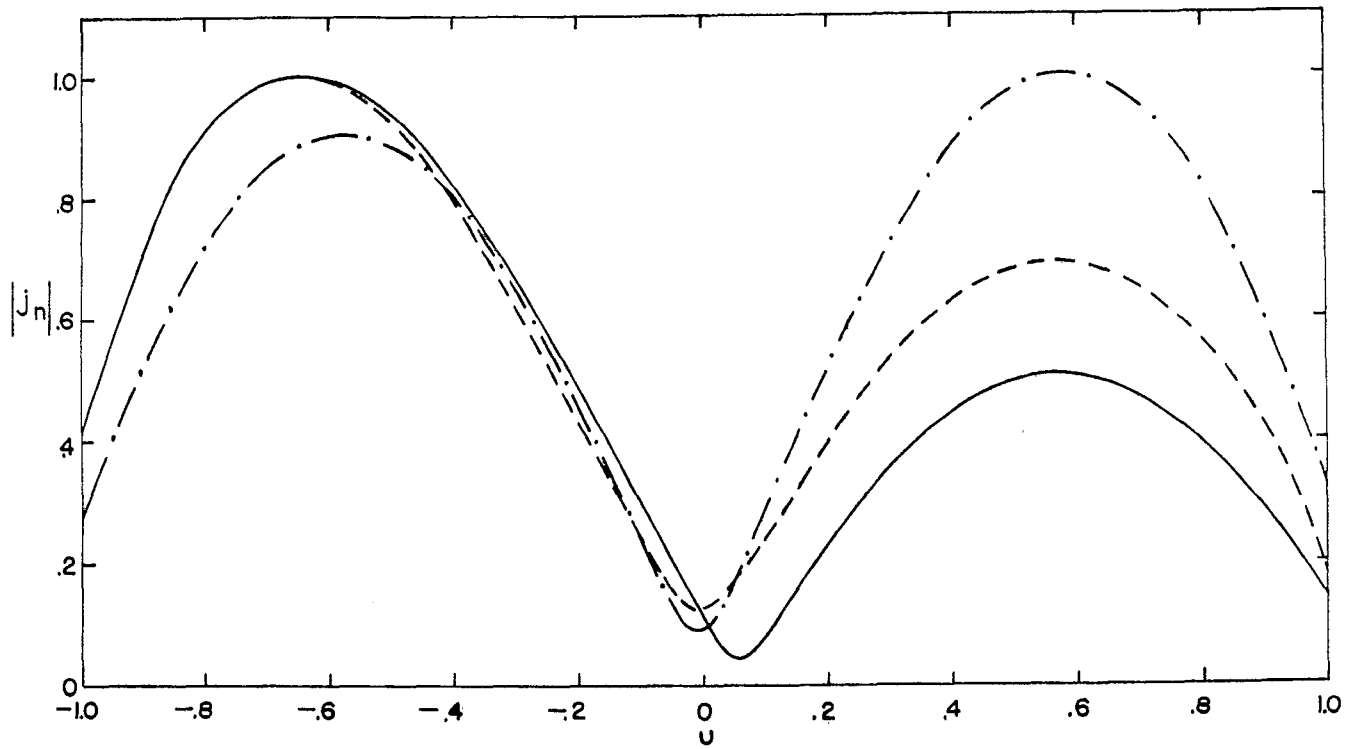
———$\gamma h = -1.094 + i2.379$;   ———————$\gamma h = -.754 + i2.891$

—··—··—$\gamma h = -.274 + i2.667$
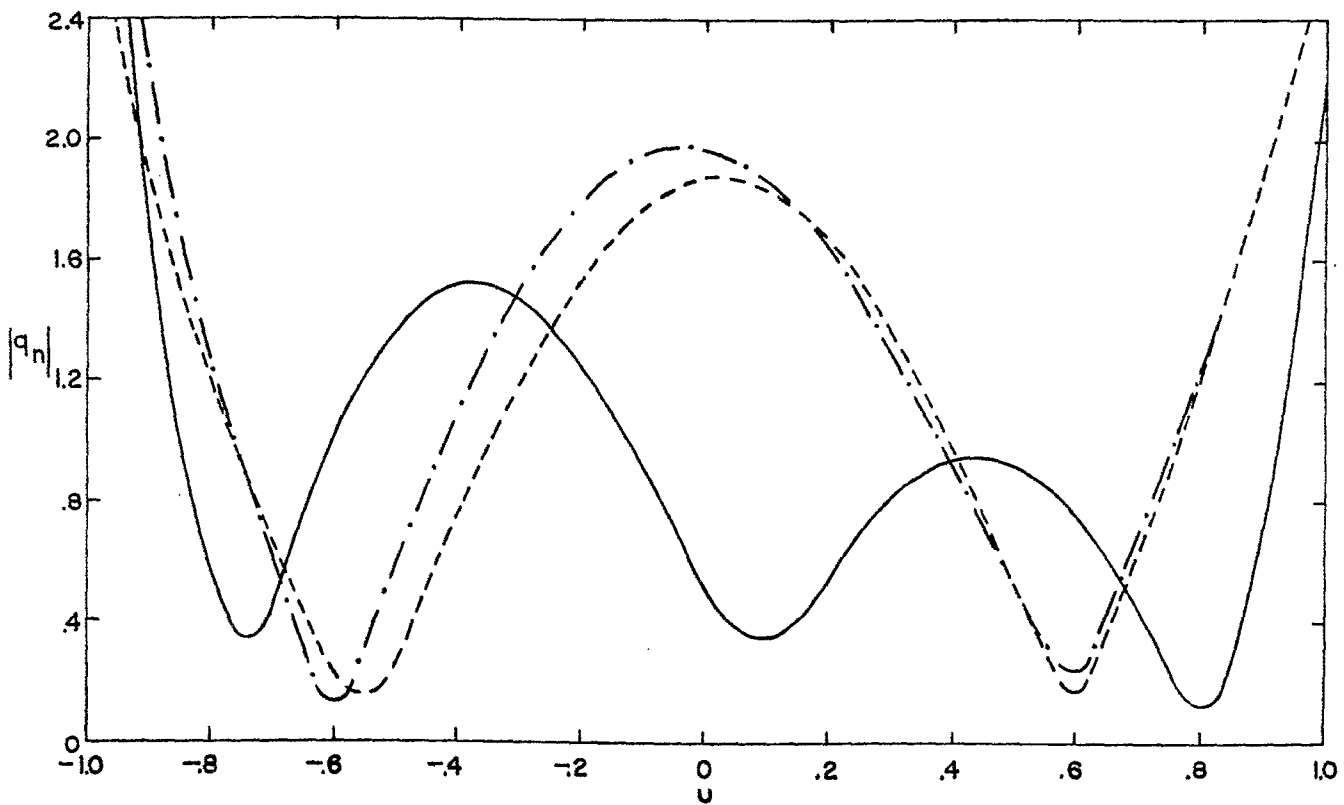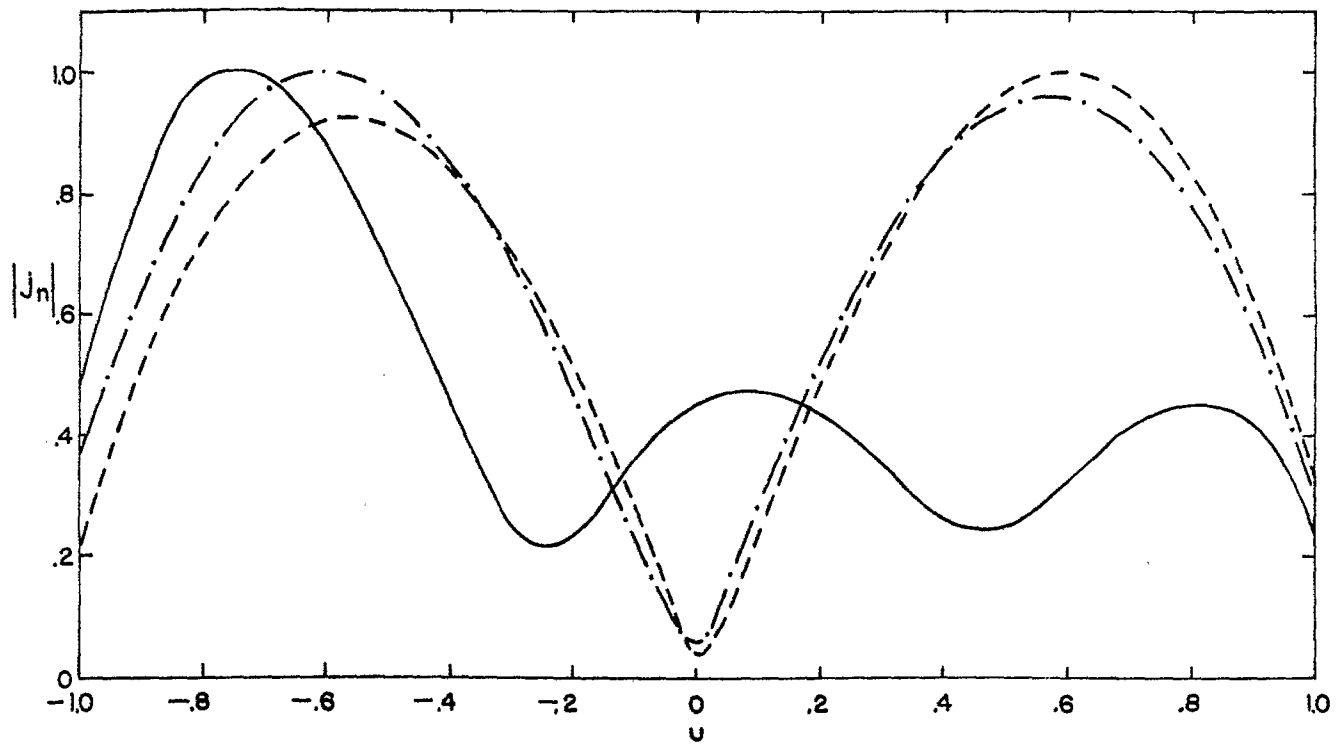
Figure 29. Current and charge distributions of the "second" natural mode for a/h = .1 and d/h = .7.

44
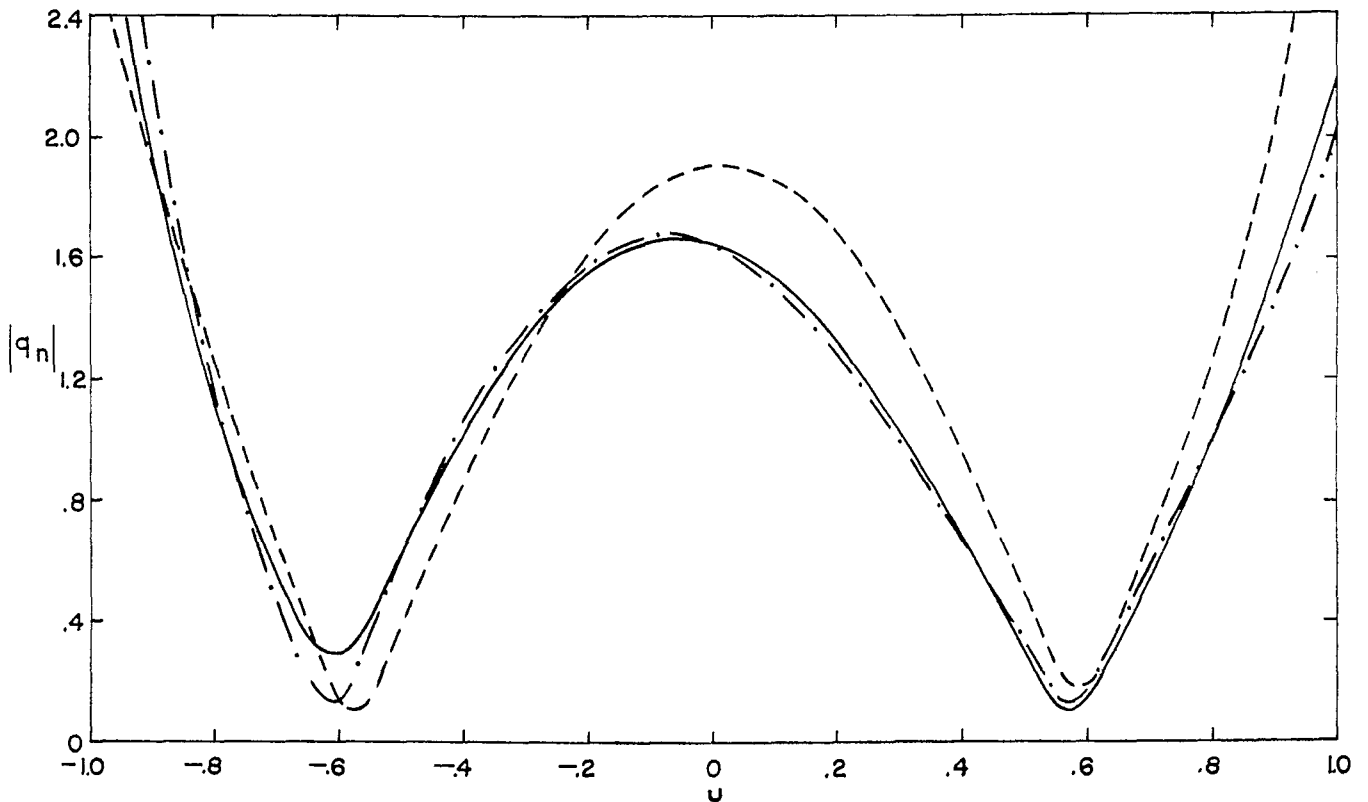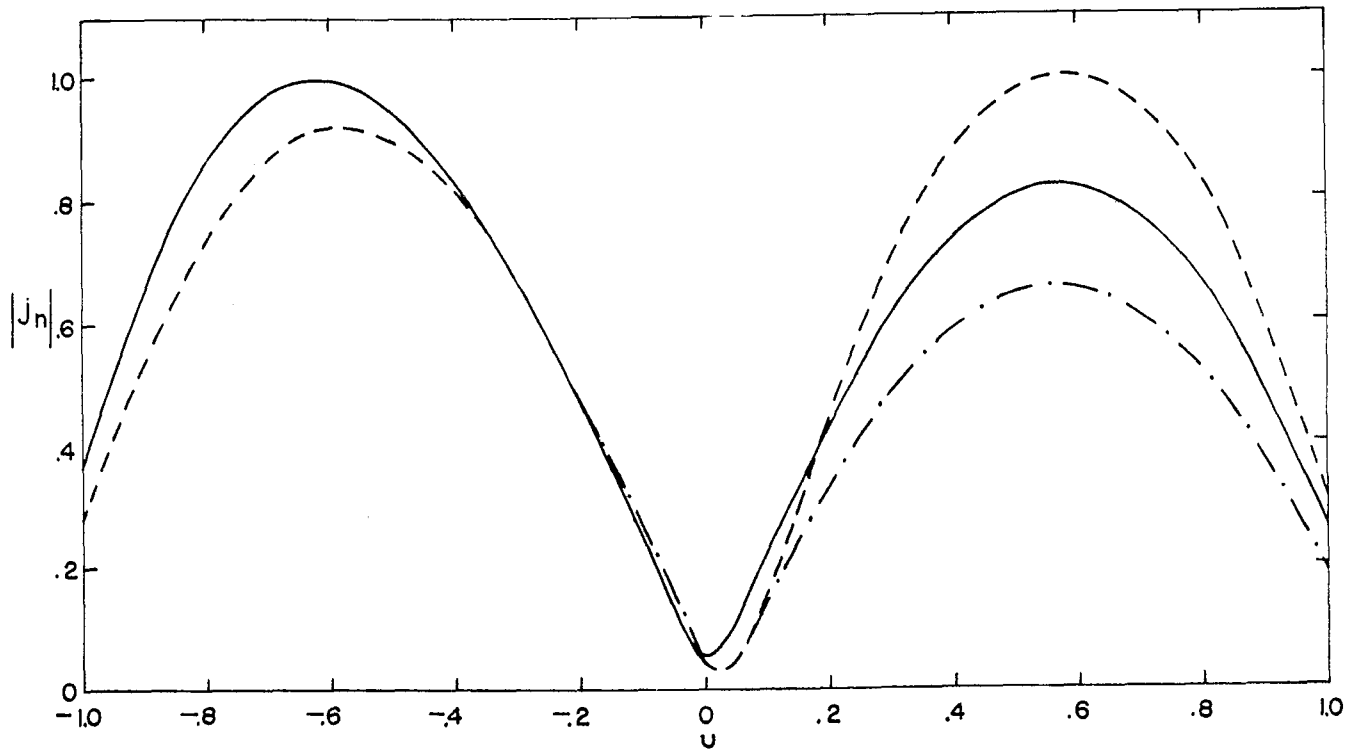
Figure 30.   Current and charge distributions of the "second" natural mode
for a/h = .1 and d/h = .9.

45

Appendix
The Natural Modes of a Thin Wire

In this appendix we will investigate analytically the natural modes of a perfectly conducting cylinder in the limiting case where the diameter-to-length ratio of the cylinder tends to zero.

Let $j(z)$ denote the part of the axial component of the current density that is independent of the azimuthal angle ϕ. The quantity $j(z)$ satisfies the differential-integral equation (the Pocklington equation)

$$\left[\frac{d^2}{dz^2} - \gamma^2\right] \int_{-h}^{h} aG(z - z')j(z')dz' = -\gamma Z_0^{-1} E_z^{inc}(z), \qquad z \in (-h,h) \qquad (A1)$$

where

$$G(\zeta) = \pi^{-1} \int_0^{\pi/2} R^{-1} \exp(-\gamma R)d\psi$$

$$R^2 = 4a^2 \sin^2\psi + \zeta^2$$

a and $2h$ being, respectively, the radius and length of the cylinder. We are interested in the nontrivial solutions of (A1) when $E_z^{inc}(z) \equiv 0$ (the homogeneous solution). For $E_z^{inc}(z) \equiv 0$ we can integrate (A1) to get

$$\int_{-h}^{h} aG(z - z')j(z')dz' = A \cosh(\gamma z) + B \sinh(\gamma z) \qquad (A2)$$

where A and B are constants of integration to be determined from the end conditions $j(\pm h) = 0$. Of course, A and B are both functions of a and h.

Next, we assume that there exists a solution of (A2) such that $j(z)$ is continuous for $-h < z < h$. Under this assumption we will investigate the left hand side of (A2) in the limit as $a \to 0$. Here and in the following $a \to 0$ actually means that $a/h \to 0$ but for simplicity we just say $a \to 0$. For that reason we split the integral in (A2) into three parts:

$$I_1 = \int_{-h}^{z-\varepsilon} aG(z - z')j(z')dz'$$

$$I_2 = \int_{z-\varepsilon}^{z+\varepsilon} aG(z - z')j(z')dz' \qquad \text{(A3)}$$

$$I_3 = \int_{z+\varepsilon}^{h} aG(z - z')j(z')dz'$$

where ε is such that $|\gamma\varepsilon| \ll 1$ but $\varepsilon \gg a$. This choice of ε is obviously possible when $a \to 0$. From (A3) it can be shown that

$$|I_1| + |I_2| < 4\pi ha\varepsilon^{-1}|j|_{max} \qquad \text{(A4)}$$

and

$$I_3 = K(\varepsilon,a)j(z) + j'(z) \qquad \text{(A5)}$$

where

$$|j'(z)| < 5\pi a\varepsilon|j|_{max}$$

and

$$K(\varepsilon,a) = 8a \int_{o}^{\varepsilon}\int_{o}^{\pi/2} (4a^2 \sin^2\psi + \zeta^2)^{-1/2} d\zeta d\psi. \qquad \text{(A6)}$$

Interchanging the order of integration in (A6) one obtains

$$K(\varepsilon,a) = -8a \int_{o}^{\pi/2} \ln\{\tan[\pi/4 - 1/2 \arctan(\varepsilon/2a \sin \psi)]\}d\psi. \qquad \text{(A7)}$$

For $\varepsilon \ll a$ we have

47

$$K(\varepsilon,a) = 4\pi a \, \ln(\varepsilon/a) + O(a/\varepsilon). \tag{A8}$$

Thus, in the limit as a → 0 (A2) has the following solution

$$j(z) = [A \cosh(\gamma c) + B \sinh(\gamma c)]/[4\pi a \, \ln(\varepsilon/a)]. \tag{A9}$$

The end conditions, $j(\pm h) = 0$, imply that

$$A \cosh(\gamma h) \pm B \sinh(\gamma h) = 0. \tag{A10}$$

The set of equations (A10) has a nontrivial solution provided that

$$\gamma = in\pi/2h. \tag{A11}$$

Therefore, the natural frequencies of a thin wire are given by (A11) and the current distribution of the natural modes are

$$j_n(z) = \begin{cases} \sin(n\pi z/2h), & n \text{ even} \\ \cos(n\pi z/2h), & n \text{ odd} \end{cases} \tag{A12}$$

The quantities $\gamma_n = in\pi/2h$ and $j_n(z)$ are represented graphically in Section IV.

48

Acknowledgment

References

1. C. E. Baum, "On the Singularity Expansion Method for the Solution of Electromagnetic Interaction Problems," Interaction Note 88, December 1971.

2. L. Marin and R. W. Latham, "Analytical Properties of the Field Scattered by a Perfectly Conducting, Finite Body," Interaction Note 92, January 1972.

3. L. Marin, "Application of the Singularity Expansion Method to Scattering From Imperfectly Conducting Bodies and Perfectly Conducting Bodies Within a Parallel Plate Region," Interaction Note 116, June 1972.

4. C. E. Baum, "On the Singularity Expansion Method for the Case of First Order Poles," Interaction Note 129, October 1972.

5. F. M. Tesche, "On the Singularity Expansion Method as Applied to Electro-magnetic Scattering From Thin Wires," Interaction Note 102, April 1972.

6. S. W. Lee and B. Leung, "The Natural Resonance Frequency of a Thin Cylinder and its Application to EMP Studies," Interaction Note 96, January 1972.

7. J. P. Martinez, Z. L. Pine and F. M. Tesche, "Numerical Results of the Singularity Expansion Method as Applied to a Plane Wave Incident on a Perfectly Conducting Sphere," Interaction Note 112, May 1972.

8. L. Marin, "Natural-Mode Representation of Transient Scattering From Rotationally Symmetric, Perfectly Conducting, Bodies and Numerical Results for a Prolate Spheroid," Interaction Note 119, August 1972.

9. S. W. Lee, V. Jamnejad and R. Mittra, "An Asymptotic Series for Early Time Response in EMP Problems," Interaction Note 128, October 1972.

10. T. H. Shumpert, "Thin Wire Over a Ground Plane Using the Singularity Expansion Method," Proceedings of the 1972 Fall Fulmen Meeting.

11. F. M. Tesche, "Application of the Singularity Expansion Method to RES Problems," Proceedings of the 1972 Fall Fulmen Meeting.

12. L. Marin, "A Cylindrical Post Above a Perfectly Conducting Plate, II (Dynamic Case)," Sensor and Simulation Note 136, August 1971.

13. L. Marin, "A Cylindrical Post Above a Perfectly Conducting Plate, I (Static Case)," Sensor and Simulation Note 134, July 1971.

14. C. E. Baum, "Interaction of Electromagnetic Fields With an Object Which has an Electromagnetic Symmetry Plane," Interaction Note 63, March 1971.